ENTPD1(CD39) expression inhibits ultraviolet radiation-induced DNA damage repair via purinergic signaling and is associated with metastasis in human cutaneous squamous cell carcinoma

[1,*]Melodi Javid Whitley, [1,*]Jutamas Suwanpradid, [2,3*]Chester Lai, [1]Simon Jiang, [1]Jonathan L. Cook, [4]Daniel E. Zelac, [5]Ross Rudolph, [6]David L. Corcoran, [1]Simone Degan, [7,8]Ivan Spasojevic,[9]Howard Levinson, [9]Detlev Erdmann, [2,3]Claire Reid, [1,10, 11]Jennifer Y. Zhang, [12]Simon C. Robson, [2,3]Eugene Healy, [13]Wendy L. Havran, and [1,10,11,14,15]Amanda S. MacLeod

[*]These authors contributed equally to this work

[1]Department of Dermatology, Duke University School of Medicine, Durham, NC, USA

[2]Dermatopharmacology, Clinical and Experimental Sciences, Faculty of Medicine, University of Southampton, Southampton, UK

[3]Department of Dermatology, University Hospital Southampton NHS Foundation Trust, Southampton, UK

[4]Division of Dermatology, Scripps Clinic and Research Institute, La Jolla, CA

[5]Division of Plastic Surgery, Scripps Clinic, La Jolla, CA and Division of Plastic Surgery, University of California, San Diego, CA (current affiliation)

[6]Center for Genomics and Computational Biology, Duke University School of Medicine, Durham, NC

[7]Department of Medicine, Duke University Medical Center, Durham, NC

[8]Duke Cancer Institute, PK/PD Core Laboratory, Durham, NC

[9]Division of Plastic, Maxillofacial, and Oral Surgery, Department of Surgery, Duke University School of Medicine, Durham, NC

[10]Pinnell Center for Investigative Dermatology and Skin Disease Research Center, Duke University School of Medicine, Durham, NC

[11]Duke Cancer Institute, Duke University Medical Center, Durham, NC

[12]Departments of Anesthesia and Medicine, Beth Israel Deaconess Medical Center, Harvard University, Boston, MA

[13]Department of Immunology and Microbiology, The Scripps Research Institute, La Jolla, CA

[14]Department of Immunology, Duke University School of Medicine, Durham, NC

[15]Department of Molecular Genetics and Microbiology, Duke University School of Medicine, Durham, NC

Corresponding Author:

Amanda S. (Büchau) MacLeod, M.D.

Department of Dermatology

Duke University Medical Center

Purple Zone, DUMC 3135

40 Duke Medicine Circle

Durham, NC 27710

Email: Amanda.MacLeod@duke.edu

Phone: 001 919 684 2074

Short Title: ENTPD1 expression in cutaneous squamous cell carcinoma

ORCID IDs:

Melodi Javid Whitley: 0000-0002-8163-6881
Jutamas Suwanpradid: 0000-0002-7933-5588
Chester Lai: 0000-0003-2282-5655
Simon Jiang: 0000-0002-9509-9001
Jonathan L. Cook: 0000-0002-8754-7900
Daniel E. Zelac: 0000-0001-5901-4544
Ross Rudolph: 0000-0002-4761-9068
David L. Corcoran: 0000-0001-7460-9247
Simone Degan: 0000-0001-5417-1196
Ivan Spasojevic: 0000-0002-3150-3087
Howard Levinson: 0000-0003-4933-4645
Detlev Erdmann: 0000-0002-3154-9368
Claire Reid: 0000-0002-9044-7572
Jennifer Y. Zhang: 0000-0002-4485-1750
Simon C. Robson: 0000-0001-6374-0194
Eugene Healy: 0000-0001-5591-6970
Wendy L. Havran: 0000-0002-1932-406X
Amanda S. MacLeod: 0000-0001-8139-9110

Abbreviations:

ADO:	adenosine
AMP:	adenosine monophosphate
ATP:	adenosine triphosphate
CLA:	cutaneous lymphocyte antigen
cSCC:	cutaneous squamous cell carcinoma
DDR:	DNA damage repair
DC:	dendritic cell
ENTPD1/CD39:	ectonucleoside triphosphate diphosphohydrolase 1
HNSCC:	head and neck squamous cell carcinoma
IHC:	immunohistochemistry
LC:	Langerhans cell
NAP1L2:	nucleosome assembly protein 1 like 2
NL:	non-lesional
Treg:	regulatory T cell
UVR:	ultraviolet radiation

ABSTRACT

Ultraviolet radiation (UVR) and immunosuppression are major risk factors for cutaneous squamous cell carcinoma (cSCC). Regulatory T cells (Tregs) promote cSCC carcinogenesis and in other solid tumors, infiltrating Tregs and $CD8^+$ T cells express ENTPD1 (*also known as* CD39), an ecto-enzyme that catalyzes the rate-limiting step in converting extracellular ATP to extracellular adenosine. We previously demonstrated that extracellular purine nucleotides influence DNA Damage Repair (DDR). Here we investigate whether DDR is modulated via purinergic signaling in cSCC. We found increased ENTPD1 expression on T cells within cSCCs when compared to T cells from blood or non-lesional skin and accordingly, concentrations of derivative extracellular ADP, AMP, and adenosine are increased in tumors compared to normal skin. Importantly, ENTPD1 expression is significantly higher in human cSCCs that metastasize compared to those that are non-metastatic. We also identify in a mouse model that ENTPD1 expression is induced by UVR in an IL27-dependent manner. Finally, increased extracellular adenosine is shown to downregulate the expression of *NAP1L2*, a nucleosome assembly protein we show to be important for DDR secondary to UVR. Together, these data suggest a role for ENTPD1 expression on skin-resident T cells to regulate DDR via purinergic signaling to promote skin carcinogenesis and metastasis.

INTRODUCTION

Ultraviolet radiation (UVR) causes inflammatory, immunosuppressive and genotoxic responses. UVR exposure and immunosuppression are major risk factors for cutaneous squamous cell carcinoma (cSCC), one of the most common cancers in the world (Que et al., 2018). UVR initiates a cascade of inflammatory events that modify the innate and adaptive immune system in the skin to allow for tumor initiation, proliferation, invasion, and spread. In human cSCC, this response is characterized by tumor-infiltrating immunosuppressive cells, i.e. tolerogenic T cells (Lai C, 2015). However, the underlying molecular mechanisms and consequences of such changes are not known.

In healthy skin, resident immune cells function to protect against environmental damage by regulating repair functions and providing long-term immune surveillance. UV-induced DNA damage in cells may be repaired by specialized repair machineries that work in concert with chromatin-associated elements to access and repair DNA lesions. We and others have previously shown that skin-resident immune cells are unexpected but relevant contributors to the DNA damage repair (DDR) response in keratinocytes following acute UVB exposure (MacLeod AS, 2014, Majewski et al., 2010) . This effect is partly attributed to the release of skin immune cell-derived cytokines that induce DDR genes in keratinocytes. Specifically, we previously demonstrated that extracellular ATP (eATP) activates murine dendritic epidermal $\gamma\delta$ T cells and human skin-resident T cells to promote epithelial DDR following acute UVB-induced damage (MacLeod AS, 2014). This protective pathway may become suppressed during skin carcinogenesis as repeated UVR insults and defective DDR result in genomic instability and a tumor-promoting microenvironment (Harberts et al., 2015).

Purinergic signaling describes the effects mediated by eATP and derivative metabolites. Important modulators of purinergic signaling are the ectonucleotidases ENTPD1 (ectonucleotidase triphosphate diphosphohydrolase 1, *also known as* CD39) and CD73 (5'-nucleotidase). ENTPD1 and CD73 catalyze the stepwise hydrolysis of ATP to metabolites ADP, AMP, and adenosine (ADO). ENTPD1 is the rate-limiting enzyme in this reaction, scavenging eATP to limit excessive inflammation. Extracellular ATP is often high in the tumor microenvironment due to increased release in response to cellular stress. This promotes anti-tumor immunity via activation of the NLRP3 inflammasome (de Andrade Mello et al., 2017). Conversely, ENTPD1 and CD73 expression are markers of regulatory T cells and contribute to their inhibitory function (Deaglio et al., 2007). Furthermore, persistent ENTPD1 upregulation on tumor infiltrating lymphocytes, which metabolizes eATP leading to increased concentration of eADO, is often seen in cancer (Canale et al., 2018). Here, immune cells receive excessive adenosinergic signals that activate A2A-receptors to trigger immunosuppression. This immunosuppressive function of adenosine has been associated with loss of anti-tumor killing activities, but putative roles in the regulation of DDR in the setting of carcinogenesis have not been studied.

Here, we explore the role of ENTPD1 expression by tumor infiltrating immune cells in regulating DDR via purinergic signaling to promote UVR-induced carcinogenesis. We report that UVB may activate IL-27 signaling to boost generation of $ENTPD1^+$ skin-homing memory T cells and $CD14^+$ myeloid cells. ENTPD1 on these immune cells facilitates metabolism of eATP and generation of adenosine within human cSCC. We show eADO-mediated downregulation of DDR, thereby, elucidating the activation and downstream effects of the ENTPD1/CD73 immune checkpoint in UVR-induced human cSCC.

RESULTS

Increased expression of ectonucleotidases ENTPD1 and CD73 on cSCC peritumoral stromal cells. Human cSCC tumors displayed significantly elevated levels of *ENTPD1* mRNA and protein expression, when compared to unmatched normal healthy skin derived from plastic surgery procedures (**Figure 1A, B and Figure S1**). ENTPD1 expression among tumor-infiltrating immune cells, as measured by immunohistochemistry (IHC), was higher in tumors that metastasized compared to those that did not (**Figure 1C**). ENTPD1 was predominantly expressed by the $CD45^+$ immune cell infiltrate, with minimal expression on $CD45^-$ epithelial and endothelial cells (**Figure 1D**). Immunofluorescence of human cSCC shows ENTPD1 expression in the adjacent peritumoral stroma (**Figure 1E**).

$CD45^+ENTPD1^+$ cells are majorly comprised of two subsets, $CD3^+$ T cells and $CD14^+$ cells that represent a heterogeneous population of macrophages and monocyte-derived macrophages (**Figure S2A, B)**. The frequency of $ENTPD1^+CD3^+$ T cells is significantly higher in cSCC when compared to adjacent non-lesional (NL) skin and peripheral blood (**Figure 1F**). The frequency of $ENTPD1^+CD14^+$ cells is high among all tissues types (**Figure S2C**) consistent with previous reports showing ENTPD1 expression on bone marrow derived monocytes (Cohen et al., 2013). On the other hand, intratumoral expression of the ecto-5'-nucleotidase CD73, which functions downstream of ENTPD1 to generate adenosine, is primarily on endothelial cells with progressively less expression on $CD14^+$ and T cells, respectively (**Figure S2D).**

In agreement with previous reports, and a reanalysis of microarray gene expression data from McGovern et al (McGovern et al., 2014) and Haniffa et al (Haniffa et al., 2012), ENTPD1 is expressed distinctly by epidermal and dermal dendritic cells (DCs) and macrophage subsets in healthy skin and we detected high expression of ENTPD1 on Langerhans cells (LCs), i.e.

epidermal CD1a$^+$ cells, in healthy skin (Kansas et al., 1991, Mizumoto et al., 2002) (**Figure S3A**). However, we also observed a reduction of the CD1a$^+$ DC population in several human cSCCs, in accordance with previously published results (**Figure S3B**) (Bluth et al., 2009). In contrast, ENTPD1-expressing CD14$^+$ cells were present in all human cSCC analyzed (**Figure S2B, D and S3B**). These cSCC-associated CD14$^+$ cells express variable levels of CD73 and consistently CD36, CD206, DC SIGN and the cutaneous lymphocyte antigen (CLA) (**Figure S3C**).

Human cSCC are enriched with ENTPD1-expressing skin resident memory T cells. Once we established that ENTPD1 expression was primarily enhanced on peritumoral T cells, we examined expression of ENTPD1 on distinct T cell subsets. Interestingly, increased ENTPD1 expression in cSCC was observed on CD8$^+$ and CD4$^+$FoxP3$^-$ effector T cells as well as CD4$^+$FoxP3$^+$ regulatory T cells (Tregs), where ENTPD1 expression has been previously reported (**Figure 2A-D**) (Borsellino et al., 2007). Across the studied T cell subsets, the expression of ENTPD1 was increased on tumor-adjacent non-lesional (NL) skin and cSCC tumor tissue compared to peripheral blood. Specifically, we observed a gradient of FoxP3$^+$ENTPD1$^+$ cell enrichment when comparing peripheral blood, NL and cSCC, respectively (**Figure 2E**). Among the ENTPD1$^+$CD4$^+$ and CD8$^+$ T cells witin the primary tumor, NL skin, and blood, expression of CD45RO was overall high, indicating that the majority of ENTPD1-expressing T cells in cSCC patients are memory T cells (**Figure 2F, G**). Notably, these CD45RO$^+$ENTPD1$^+$ cells were enriched at the primary cSCC site compared to T cells isolated from blood or NL skin from the same patient (**Figure 2H**). Among memory T cells, FoxP3 expression was highest in cSCC and lowest in peripheral blood with intermediate expression in NL (**Figure 2I**). ENTPD1

expression on CD45RO+ memory T cells however, is relatively independent of tissue type (**Figure 2J**).

Normal human skin contains >90% memory T cells, of which almost all express CLA, critical for skin-homing (Clark et al., 2006). In contrast, CLA is expressed on only 10-25% of circulating memory T cells in healthy individuals (Clark et al., 2006). Notably, the majority of ENTPD1$^+$ T cells in cSCC and healthy or non-lesional skin from cSCC patients were CLA$^+$, whereas the majority of ENTPD1$^-$ T cells were CLA$^-$ (**Figure 3A).** Among ENTPD1-expressing CD4$^+$ and CD8$^+$ T cell subsets, the majority of T cells present in NL or cSCC skin were CLA$^+$ and this frequency was significantly higher compared to T cells in the blood of respective cSCC patients (**Figure 3B, C**).

PD-1 and ENTPD1 are co-expressed on FoxP3$^-$ memory T cells within human cSCC. Given that immune-inhibitory molecules often synergize to confer maximal inhibitory functions (Pardoll, 2012), we tested the possibility that ENTPD1 and PD-1 may be co-expressed. PD-1 and its two ligands, PD-L1 and PD-L2, have been previously identified in multiple cancers, including cSCC. We find that PD-1 was expressed by approximately 50% of T cells in human cSCC (**Figure 4A**). About 1/5 of T cells within human cSCC co-expressed PD-1 with ENTPD1 (**Figure 4B**). As expected, the expression pattern of PD-1 was highly distinct between FoxP3$^-$ and FoxP3$^+$ T cell subsets. Within the FoxP3$^-$ T cell subset, but not within the FoxP3$^+$ T cell subset, PD1$^+$ENTPD1$^+$ T cells were highly elevated in cSCC compared to T cells in NL skin and blood (**Figure 4C**).

IL-27 promotes ENTPD1 and FoxP3 expression on human skin-resident T cells. IL-27, comprised of IL-27p28 (IL-27A) and Epstein-Barr Virus-induced gene 3 (EBI3), is produced abundantly by activated myeloid cells (Mascanfroni et al., 2013) and signals through the IL-27 receptor comprised of IL27RA and IL27RB. The IL-27 receptor complex is widely expressed on myeloid cells and T cells (Pflanz et al., 2004). IL-27 directly blocks T-cell responses through up-regulation of IL-10 and ENTPD1 on dendritic cells and indirectly through induction of PD-L1 and ENTPD1 (Mascanfroni et al., 2013, Sekar et al., 2012). Recent studies highlight that IL-27 enhances Treg accumulation and immunosuppressive function (Sekar et al., 2012, Xia et al., 2014). We found that IL27A expression is increased in human cSCC compared to normal skin and co-localized with CD209 (*also known as* DC-SIGN) expression (**Figure 5A-D**). IL-27A is sufficient to induce ENTPD1 on human T cells (**Figure 5E**). Furthermore, IL-27A induces FoxP3 expression, supporting its role as an enhancer of Treg accumulation (**Figure 5E**).
As described above, we noted that ENTPD1 expression is increased not only in cSCCs but also in chronically sun-exposed NL skin, suggesting that UVR may induce ENTPD1 expression. To determine the role for IL-27 signaling in UVR-induced ENTPD1 expression, we exposed WT and *IL-27RA*$^{-/-}$ mice to narrow band UVB (311-312 nm). We found that *IL-27RA*$^{-/-}$ mice have significantly lower levels of UVB-induced *Entpd1* compared to control mice (**Figure 5F, G**).

IL-27 signaling in T cells causes accumulation of UVB-induced DNA damage via ENTPD1.
Once established that UVB induces ENTPD1 expression in an IL27-dependent manner, and that this pathway is upregulated in cSCCs, we sought to determine whether this pathway influences DDR after UVR. Human skin T cells from healthy donors were treated with recombinant human IL-27, washed twice to remove any remaining IL-27, and re-stimulated with plate-bound anti-

CD3 in keratinocyte growth medium. Conditioned keratinocyte medium and control medium were collected and added to human keratinocyte cultures which were UVB-treated. Subsequently, DNA damage was measured in keratinocytes by γH2AX accumulation, a commonly used marker of UV-induced DNA damage (Fernandez-Capetillo et al., 2002, Marti et al., 2006, Modi et al., 2012, Paull et al., 2000, Rogakou et al., 1998). Notably, quantification of $\gamma H2AX^+$ keratinocytes treated with T cell condition medium revealed that prior priming of skin T cells with IL-27 resulted in accumulation of epithelial DNA damage, possibly due to a defect in DDR (**Figure 6A**). Furthermore, in an *in situ* mouse ear model system, which provides a controlled model system by preventing influx of peripheral immune cells, we found that treatment of WT mouse ears with recombinant IL-27 strongly attenuated resolution of γH2AX foci in keratinocytes following UVB-irradiation (**Figure 6B**). This response was lost in mice deficient in *Il27ra* or *Entpd1*. Finally, we found that ENTPD1 expression co-localizes with areas of high DNA damage within cSCCs (**Figure 6C**) and peritumoral skin (**Figure 6C, D and Figure S4**). Together, our data is highly suggestive that IL-27 affects T cells to cause accumulation of UVB-induced DNA damage via ENTPD1.

Extracellular adenosine downregulates expression of putative keratinocyte DNA repair protein(s). We then turned our attention to how IL27-mediated UV-induced ENTPD1 expression on skin resident memory T cells may modulate DDR in keratinocytes. ENTPD1 functions to increase the local concentration of extracellular adenosine (eADO). We found that indeed, the concentration of extracellular ATP metabolites including adenosine is higher in cSCC samples when compared to normal skin (**Figure S5**). To determine the effect of eADO on keratinocyte gene expression, we stimulated keratinocytes with either vehicle or 10 μM

adenosine, and report the 49 probes with the most significantly different expression after 24 hours (**Figure 6E**).

There was differential expression of several genes previously implicated in DDR. Downregulated genes with known DDR functions included *TNFAIP3* (Yang et al., 2018), *EGR1* (Thyss et al., 2005), *LIF* (Liu et al., 2014), *NAP1L2* (Gao et al., 2012), and *KRT23* (Birkenkamp-Demtroder et al., 2013). Upregulated proteins with known DDR functions included *MSH6* (Edelbrock et al., 2013), *AKR1B10* (Shen et al., 2015), and *HERC5* (Sanchez-Tena et al., 2016). *TNFRSF10C*, which is a known p53-regulated DNA damage-inducible gene, was upregulated with adenosine treatment (Sheikh et al., 1999). Interestingly, several genes involved with viral pathogenesis including *PEG10*, *MX1*, *IFI44*, and *DDX60* were upregulated after treatment with adenosine (Berard et al., 2015, Kaczkowski et al., 2012). Finally, adenosine treatment induced the expression of several genes implicated in the interferon gene response (*IRF9*, *MX1*, *IFIT1*) (Gerner et al., 2019).

We further investigated the adenosine-mediated downregulation of *NAP1L2*, or nucleosome assembly protein 1 like 2. *NAP1L2* is a member of the nucleosome assembly protein (NAP) family with known functions that include nucleosome assembly, histone transport, histone eviction, transcriptional regulation and cell cycle progression (Attia et al., 2011). Nucleosome assembly and histone chaperones are an integral element of nucleotide excision repair, which is the primary mode of repair for UV-induced cyclobutane pyrimidine dimers and pyrimidine (6-4) pyrimidone photoproducts (Palomera-Sanchez and Zurita, 2011). Recent studies have also shown a role for NAP1 in the repair of DNA double strand breaks (Machida et al., 2014) which often occur secondary to UVA radiation.

We confirmed adenosine-mediated NAP1L2 downregulation in the A431 SCC cell line. We found significant downregulation of NAP1L2 at the transcript and protein level when cells were treated with 10 μM adenosine for 24 and 48 hours, respectively (**Figure 6F, G)**.

To determine whether *NAP1L2* expression is necessary for effective repair of UV-induced DNA damage in keratinocytes, we expressed a siRNA against *NAP1L2* in human keratinocytes. The keratinocytes were UV-irradiated and the extent of DNA damage, as marked by 53BP1 expression, was measured at 2 and 24 hours. We found that detection of 53BP1-positive foci increased at two hours after UV exposure regardless of *NAP1L2* expression. At 24 hours, however, *NAP1L2* knockdown resulted in accumulation of DNA damage, while the cells treated with control siRNA were able to effectively clear any acute damage (**Figure 6F**).

Together, our results demonstrated that IL-27-mediated UV-induced ENTPD1 expression and downstream increase in eADO suppresses DDR. This is directly linked to the capacity of eADO to downregulate expression of NAP1L2, a putative member of the DNA repair machinery, in keratinocytes and a cSCC tumor cell line. Notably, T cells in close proximity to human cSCC are characterized by high ENTPD1 expression, implicating that our identified mechanisms could also apply to human cSCCs.

DISCUSSION

The risk factors for developing cSCC are well known and include age, sun exposure, skin type and immunosuppression (Que et al., 2018). UVB radiation induces DNA damage within keratinocytes that accumulates with increased sun exposure and age. Importantly, both clinical and laboratory investigations have revealed an important role for innate and adaptive immunity in cSCC carcinogenesis (Bottomley et al., 2019).

The current paradigm suggests that cancer cells and the associated microenvironment suppress immune surveillance function. Currently, it is not well understood whether and how the immune status can *a priori* regulate mechanisms of oncogenesis such as UV-induced DNA damage and DDR. Recently, work from Girardi and colleagues on dendritic cells (Lewis et al., 2015) and our work on skin T cells has explored this area. Notably, we previously made the discovery that upon acute UV damage, skin-resident T cells increase epithelial TWEAK and GADD45 to stimulate early DDR (MacLeod AS, 2014). In contrast, here we report a pathway in which UV radiation induces expression of ENTPD1 on regulatory T cells to impair DDR.

In this study, we show that ENTPD1 expression by tumor associated T cells is higher in human primary cSCCs when compared to normal skin. This phenotype is observed in human tumors from disparate geographic sites, including both the west and east coasts of the USA as well as the United Kingdom. We also show here that ENTPD1 expression may be associated with metastatic potential of cSCC. This is in line with many studies that have shown tumor-specific increased expression of ENTPD1 in other solid tumors, including head and neck SCC (HNSCC), and suggest ENTPD1 expression may be associated with worse prognosis (Mandapathil et al., 2018, Mandapathil et al., 2009, Vigano et al., 2019).

Importantly, we show that these ENTPD1 expressing T cells have a predominantly CLA^+, $CD45RO^+$, $FoxP3^+$ phenotype suggesting that these are skin-homing Tregs. Interestingly, we also observe co-expression with the immune checkpoint molecule PD-1 on $FoxP3^-$ T cells. Although both ENTPD1 and PD-1 expression are classically associated with $FoxP3^+$ Tregs, others have also reported a distinct $CD4^+ENTPD1^+PD\text{-}1^+FoxP3^-$ phenotype in tumors and peripheral blood from patients with HNSCC (Schuler et al., 2012). ENTPD1 and PD-1 co-expression is thought to be a signature of T cell exhaustion (Mohme et al., 2018), emphasizing the significance of purinergic signaling in mediating the immunosuppressive activity of T cells. Furthermore, recent studies in mouse models of solid tumors have shown that dual blockade of ENTPD1 and PD-1 may provide improved tumor growth restriction and control of metastasis compared to monotherapy (Li et al., 2019, Yan et al., 2020). Investigating this approach in models of advanced cSCC will be an important next step.

In examining ENTPD1 expression on tumor infiltrating lymphocytes, we observed a gradient of expression, with enriched ENTPD1 within the perilesional NL skin compared to peripheral blood. Increased ENTPD1 expression may lead to an accumulation of UV-induced DNA damage as we and others have shown that peritumoral normal skin harbors many UV-induced oncogenic mutations (Albibas et al., 2018, Chitsazzadeh et al., 2016). Furthermore, several studies demonstrate that the mutational burden increases along the oncogenic march from actinic keratosis to cSCC (Borden et al., 2019, Chitsazzadeh et al., 2016). As Dlugosz, Merlina, and Yuspa summarized in 2002, pre-malignant lesions such as actinic keratoses often harbor evidence of UV-induced DNA damage while genomic instability is a hallmark of frank carcinoma (Dlugosz et al., 2002). Thus, increased ENTPD1 expression and subsequent down regulation of DDR may contribute to the genomic instability that characterizes cSCC. UVR has

also been shown to create a locally immunosuppressed microenvironment, specifically by inducing Tregs (Toda et al., 2011). Lai et al showed that Tregs accumulate in premalignant lesions, further supporting the role for immunosuppression in tumor initiation (Lai et al., 2016). Our work supports a role for UV-mediated induction of ENTPD1 expression in the tumor microenvironment, including cutaneous Tregs and other cell types. Others have shown induction of ENTPD1 expression by Tregs in the blood after extracorporeal UVA photophoresis (Schmitt et al., 2009). Specifically, we show that UVB-mediated ENTPD1 induction is likely mediated by IL-27 expressed by dermal myeloid cells. Previous studies have demonstrated that UVR induced keratinocyte damage results in the release of double stranded RNA that can act as a damage-associated molecular pattern to active the innate immune response via the toll-like receptor 3 (Bernard et al., 2012). We have previously published that activation of the toll-like receptor 3 with double stranded RNA results in potent stimulation of IL27 expression by dermal myeloid cells (Yang et al., 2017). The murine studies presented here demonstrate that UV induction of ENTPD1 expression is dependent on the presence of a functional IL27 receptor. Importantly, in 2013 Mascanfroni et al showed that IL27 is a potent inducer of ENTPD1, resulting in decreased extracellular ATP (Mascanfroni et al., 2013). Together, these data demonstrate that IL27-mediated ENTPD1 induction is an important mechanism of UV-induced immunosuppression. We go on to show that ENTPD1 expression localizes to areas of DNA damage to impair DDR. ENTPD1 is the rate-limiting step in generating adenosine that signals through cell surface receptors to promote regulatory T cells and suppress effector T cell function (de Andrade Mello et al., 2017). Here we show a novel mechanism by which purinergic signaling may regulate DDR to promote cSCCs.

Interestingly, others have proposed a role for purinergic signaling in DDR following ionizing radiation. Tsukimoto and others have shown that extracellular ATP may signal through P2X and P2Y receptors to result in accumulation of DNA damage (Tsukimoto, 2015). ADO on the other hand, signals through the G-protein coupled receptors A_1R, $A_{2A}R$, $A_{2B}R$ and A_3R to result in accumulation of cyclic AMP and downstream suppression of T-cell responses. Recently, it has been shown that HNSCC tumor cells express $A_{2A}R$ and that this molecule may serve as a therapeutic target (Vogt et al., 2018). This strongly suggests an important role for ADO receptor signaling in cSCC oncogenesis to be explored in future studies.

Here, we show that extracellular adenosine modulates the expression of several DDR-implicated genes including *NAP1L2*. NAP1L2 has been shown to serve as a H2A/B chaperone (Mazurkiewicz et al., 2006). NAPs facilitate incorporation of histone H2A/H2B dimers to complete nucleosome assembly and play critical roles in DNA repair. Furthermore, adenosine can activate caspase-3, which sub-lethally promotes persistent DNA damage and oncogenic transformation (Wen and Knowles, 2003). A recent study by Rokunohe et al, suggests that caffeine, a known adenosine receptor antagonist (Peleli et al., 2017), may reduce the burden of UV-induced mutations (Rokunohe et al., 2019), further supporting a role for purinergic signaling in regulating DDR. Given that we identified a pathway by which IL-27-induced ENTPD1 signaling promotes genomic instability in the skin, ongoing studies are underway to determine how this pathway may be therapeutically targeted in skin cancer. Our studies may also provide important insight into other cancers characterized by high ENTPD1 expression.

The experiments shown here primarily support a role for UV-induced ENTPD1 expression in promoting early events in cSCC carcinogenesis, however, we also show ENTPD1 expression to be higher in tumors that metastasize. Although this may ultimately reveal a distinct pathway of

ENTPD1 function, defective DDR and mutational status have also been implicated in the aggressiveness of SCC (Inman et al., 2018).

In conclusion, we propose a model in which UV radiation induces ENTPD1 expression on skin-resident T cells, increasing levels of extracellular adenosine which downregulates the expression of *NAP1L2* within keratinocytes leading to the accumulation of DNA damage and subsequent oncogenesis.

MATERIALS AND METHODS

Human tissue and cells. All human samples for this study were obtained according to protocols approved by the IRB at Duke University, University of Southampton (UK), and Scripps Research Institute, CA and as described in the supplemental materials and methods. Written informed consent was received from patients as required by the relevant protocols.

Normal human keratinocytes were purchased from (Cascade Biologics) and the A431 cell line were purchased from ATCC with experimental conditions as described in supplemental materials and methods.

Mouse experiments. All mice were bred and studies performed at Duke University and The Scripps Research Institute according to protocols approved by Institutional Animal Care and Use Committees (IACUC) guidelines and described in the supplemental materials and methods.

Ultraviolet Irradiation. Mice and cells were irradiated with an EB-280C/12 UVB lamp (100 mJ/cm^2, Spectroline, predominant emission 312 nm, 270-390 emission range).

Immunofluorescence. For histological analysis of epidermal ear sheets, monolayer human keratinocytes and frozen skin section, tissues and cells were paraformaldehyde-fixed and incubated in a blocking solution of PBS containing 2.5% normal goat serum (Jackson Immuno

Research), 2.5% normal donkey serum (Jackson Immuno Research), 1% bovine serum albumin (Calbiochem), 2% fish gelatin (Sigma), and 0.1% Triton-X100 for 1 hour at room temperature before overnight incubation with primary antibodies or appropriate IgG controls at 4°C. Primary antibodies used were NAP1L2 (Thermo), γH2AX (Active Motif), IL27A (LifeSpan Biosciences), ENTPD1/CD39, CD207 and CD209. Secondary antibodies were Alexa Fluor 555 (Invitrogen), Alexa Fluor 488 (Invitrogen) or Cy3-conjugated (Jackson ImmunoResearch Laboratories). After washing, sections were mounted with Prolong Gold antifade containing DAPI (Invitrogen) or Hoechst staining (Life Technologies). To quantify CD39 expression, representative images of the cSCC peritumoral immune infiltrate were obtained. The total number of immune cells and the number of $ENTPD1^+$ immune cells were counted in five high power fields per sample using technology-assisted image analysis.

Flow cytometry and fluorescence-activated cell sorting. Antibodies and appropriate IgG controls were conjugated to FITC, AF488, PE, PerCP-Cy5.5, Pe-Cy7, Pacific blue, AF780, APC-Cy7, BV421, or APC. Antibodies to mouse Vγ3 (536), TCRβ (H57-597), CD4 (GK1.5) and pan-γδTCR (GL-3),Thy1.2 (53-2.2), CD3 (HIT3a, 17A2 and 145-2C11), CD45 (HI30), IL-17A (ebio64DEC17), CD8 (53-5.8) and CD69 (H1.2F3) were purchased from TONBO, eBioscience, Biolegend, and BD Bioscience. Antibodies to human CD45, CD3, CD4, CD8, CD45R0, CLA, ENTPD1, CD73, CD11b, CD11c, CD206, DC-SIGN, PD-L1, PD-L2, PD-1, γδTCR, FoxP3, IL17A were purchased from TONBO, eBioscience, Biolegend, R&D and BD Bioscience. For detection of intracellular IL-17A, human skin T cells were stimulated with IL-27 (100 ng/ml) and were re-stimulated with PMA (2 ng/ml) and ionomycin (1μM) in the presence of brefeldin A (5μl/ml) and monensin (eBioscience, 1:1000), before cells were fixed and permeabilized with cytofix and cytoperm reagents from BD Bioscience. Cells were acquired on a

LSRII and analyzed with FlowJo software (Tree Star, Inc.). For some experiments, human myeloid cells were purified by FACS-sorting.

Real-Time PCR. Total RNA was isolated from cells using RNeasy Micro Kit (Qiagen) or from tissue using TRIzol (Invitrogen). RNA was reverse transcribed using the iScript cDNA Synthesis Kit (BioRad) and resulting cDNA was amplified using FastStart Universal SYBR Green Master Mix (Roche). Fold induction of gene expression was normalized to housekeeping gene and calculated using the $2^{(-\Delta\Delta Ct)}$ method.

Liquid chromatography – electrospray tandem mass spectrometry (LC-ESI-MS/MS). ATP, ADP, AMP, and ADO measurement was performed by the Duke Cancer Institute PK/PD Core laboratory using LC-ESI-MS/MS. Pure standards of ADO, ADO13C5, AMP, ADP, ATP (Sigma-Aldrich) and ATP15N5 (TRC) were of analytical purity. Methods from Goutiera et al. (Goutier et al., 2010) were modified as described in supplemental methods to accommodate additional metabolites and available instrumentation.

Microarray data analysis. Microarray datasets from Padilla et al. (GSE2503) (Padilla et al., 2010), Haniffa *et al* (GSE35457) (Haniffa et al., 2012) and McGovern *et al* (GSE60317) (McGovern et al., 2014) were downloaded from the Gene Expression Omnibus. For the two Illumina array datasets (Haniffa *et al* and McGovern *et al*), we applied quantile normalization from the preprocessCore Bioconductor package to eliminate systematic differences across the samples. Differential expression across groups within each dataset was calculated using an empirical Bayes' moderated test statistic using the limma Bioconductor package in the R statistical programming environment. The false discovery rate (FDR) was used to correct for multiple hypothesis testing. Human Affymetrix microarray datasets were processed and normalized using the affy and limma Bioconductor packages from the R statistical programming

environment. Raw data was first normalized to eliminate systematic differences across samples using the robust multi-array average approach and differential expression between ADO treated and control samples was calculated using a linear model with an empirical Bayes' estimation of the test statistic. The FDR was used to correct for multiple hypothesis testing. For display of expression in the different heatmaps, the expression values were z-score transformed across samples and genes were clustered using a correlation distance with complete linkage.

Statistics. Data in graphs are presented as means and error bars are standard error of the mean unless otherwise indicated. Statistical significance was measured using two-tailed Student t-test, matched pairs t-test, or Turkey's Multiple Comparison Test as indicated. A P value of <0.05 was considered significant.

Data Availability Statement. Datasets related to this article can be found at https://www.ncbi.nlm.nih.gov/geo/query/acc.cgi?acc=GSE165222, hosted at the NCBIs Gene Expression Omnibus (Edgar et al., 2002) with GEO Series accession number GSE165222.

CONFLICT OF INTEREST

The authors state no conflict of interest.

ACKNOWLEDGEMENTS

We thank Robert Streilein and Chuan-Yuan Li, D. Sc. for assistance with experiments and advice on data interpretation, respectively. We thank Russell P. Hall, MD for assistance with tissue collection and regulatory approval as well as advice on data interpretation.

CRediT STATEMENT

Conceptualization: MJW, JS, CL, SCR, EH, WLH, ASM; **Methodology:** MJW, JS, DLC, IS, ASM; **Software:** DLC; **Validation:** MJW, JS, DLC, IS, ASM; **Formal Analysis:** MJW, JS, DLC, ASM; **Investigation:** MJW, JS, CL, SJ, SD, IS, CR, ASM; **Resources:** JLC, DZ, RR, HL, DE, JYZ, SCR, EH, WLH, ASM; **Data Curation:** DLC; **Writing – Original Draft:** JS, ASM; **Writing – Review & Editing:** MJW, CL, DLC, JYZ, SCR, EH, WLH; **Visualization:** MJW, ASM; **Supervision:** ASM; **Project administration:** ASM; **Funding acquisition:** ASM.

REFERENCES

Albibas AA, Rose-Zerilli MJJ, Lai C, Pengelly RJ, Lockett GA, Theaker J, et al. Subclonal Evolution of Cancer-Related Gene Mutations in p53 Immunopositive Patches in Human Skin. J Invest Dermatol 2018;138(1):189-98.

Attia M, Forster A, Rachez C, Freemont P, Avner P, Rogner UC. Interaction between nucleosome assembly protein 1-like family members. J Mol Biol 2011;407(5):647-60.

Berard AR, Severini A, Coombs KM. Comparative proteomic analyses of two reovirus T3D subtypes and comparison to T1L identifies multiple novel proteins in key cellular pathogenic pathways. Proteomics 2015;15(12):2113-35.

Bernard JJ, Cowing-Zitron C, Nakatsuji T, Muehleisen B, Muto J, Borkowski AW, et al. Ultraviolet radiation damages self noncoding RNA and is detected by TLR3. Nat Med 2012;18(8):1286-90.

Birkenkamp-Demtroder K, Hahn SA, Mansilla F, Thorsen K, Maghnouj A, Christensen R, et al. Keratin23 (KRT23) knockdown decreases proliferation and affects the DNA damage response of colon cancer cells. PLoS One 2013;8(9):e73593.

Bluth MJ, Zaba LC, Moussai D, Suarez-Farinas M, Kaporis H, Fan L, et al. Myeloid dendritic cells from human cutaneous squamous cell carcinoma are poor stimulators of T-cell proliferation. J Invest Dermatol 2009;129(10):2451-62.

Borden ES, Kang P, Natri HM, Phung TN, Wilson MA, Buetow KH, et al. Neoantigen Fitness Model Predicts Lower Immune Recognition of Cutaneous Squamous Cell Carcinomas Than Actinic Keratoses. Front Immunol 2019;10:2799.

Borsellino G, Kleinewietfeld M, Di Mitri D, Sternjak A, Diamantini A, Giometto R, et al. Expression of ectonucleotidase CD39 by Foxp3+ Treg cells: hydrolysis of extracellular ATP and immune suppression. Blood 2007;110(4):1225-32.

Bottomley MJ, Thomson J, Harwood C, Leigh I. The Role of the Immune System in Cutaneous Squamous Cell Carcinoma. Int J Mol Sci 2019;20(8).

Canale FP, Ramello MC, Nunez N, Araujo Furlan CL, Bossio SN, Gorosito Serran M, et al. CD39 Expression Defines Cell Exhaustion in Tumor-Infiltrating CD8(+) T Cells. Cancer Res 2018;78(1):115-28.

Chitsazzadeh V, Coarfa C, Drummond JA, Nguyen T, Joseph A, Chilukuri S, et al. Cross-species identification of genomic drivers of squamous cell carcinoma development across preneoplastic intermediates. Nat Commun 2016;7:12601.

Clark RA, Chong B, Mirchandani N, Brinster NK, Yamanaka K, Dowgiert RK, et al. The vast majority of CLA+ T cells are resident in normal skin. J Immunol 2006;176(7):4431-9.

Cohen HB, Briggs KT, Marino JP, Ravid K, Robson SC, Mosser DM. TLR stimulation initiates a CD39-based autoregulatory mechanism that limits macrophage inflammatory responses. Blood 2013;122(11):1935-45.

de Andrade Mello P, Coutinho-Silva R, Savio LEB. Multifaceted Effects of Extracellular Adenosine Triphosphate and Adenosine in the Tumor-Host Interaction and Therapeutic Perspectives. Front Immunol 2017;8:1526.

Deaglio S, Dwyer KM, Gao W, Friedman D, Usheva A, Erat A, et al. Adenosine generation catalyzed by CD39 and CD73 expressed on regulatory T cells mediates immune suppression. J Exp Med 2007;204(6):1257-65.

Dlugosz A, Merlino G, Yuspa SH. Progress in cutaneous cancer research. J Investig Dermatol Symp Proc 2002;7(1):17-26.

Edelbrock MA, Kaliyaperumal S, Williams KJ. Structural, molecular and cellular functions of MSH2 and MSH6 during DNA mismatch repair, damage signaling and other noncanonical activities. Mutat Res 2013;743-744:53-66.

Fernandez-Capetillo O, Chen HT, Celeste A, Ward I, Romanienko PJ, Morales JC, et al. DNA damage-induced G2-M checkpoint activation by histone H2AX and 53BP1. Nat Cell Biol 2002;4(12):993-7.

Gao J, Zhu Y, Zhou WB, Molinier J, Dong AW, Shen WH. NAP1 Family Histone Chaperones Are Required for Somatic Homologous Recombination in Arabidopsis. Plant Cell 2012;24(4):1437-47.

Gerner MC, Niederstaetter L, Ziegler L, Bileck A, Slany A, Janker L, et al. Proteome Analysis Reveals Distinct Mitochondrial Functions Linked to Interferon Response Patterns in Activated CD4+ and CD8+ T Cells. Front Pharmacol 2019;10:727.

Goutier W, Spaans PA, van der Neut MA, McCreary AC, Reinders JH. Development and application of an LC-MS/MS method for measuring the effect of (partial) agonists on cAMP accumulation in vitro. J Neurosci Methods 2010;188(1):24-31.

Haniffa M, Shin A, Bigley V, McGovern N, Teo P, See P, et al. Human tissues contain CD141hi cross-presenting dendritic cells with functional homology to mouse CD103+ nonlymphoid dendritic cells. Immunity 2012;37(1):60-73.

Harberts E, Zhou H, Fishelevich R, Liu J, Gaspari AA. Ultraviolet radiation signaling through TLR4/MyD88 constrains DNA repair and plays a role in cutaneous immunosuppression. J Immunol 2015;194(7):3127-35.

Inman GJ, Wang J, Nagano A, Alexandrov LB, Purdie KJ, Taylor RG, et al. The genomic landscape of cutaneous SCC reveals drivers and a novel azathioprine associated mutational signature. Nat Commun 2018;9(1):3667.

Kaczkowski B, Rossing M, Andersen DK, Dreher A, Morevati M, Visser MA, et al. Integrative analyses reveal novel strategies in HPV11,-16 and -45 early infection. Sci Rep 2012;2:515.

Kansas GS, Wood GS, Tedder TF. Expression, distribution, and biochemistry of human CD39. Role in activation-associated homotypic adhesion of lymphocytes. J Immunol 1991;146(7):2235-44.

Lai C AS, Behar R, Polak, M, Ardern-Jones M, Theaker J, Al-Shamkhani A, Healy E. Characteristics of immunosuppressive regulatory T cells in cutaneous squamous cell carcinomas and role in metastasis. Lancet 2015;385(Suppl 1):S59.

Lai C, August S, Albibas A, Behar R, Cho SY, Polak ME, et al. OX40+ Regulatory T Cells in Cutaneous Squamous Cell Carcinoma Suppress Effector T-Cell Responses and Associate with Metastatic Potential. Clin Cancer Res 2016;22(16):4236-48.

Lewis JM, Burgler CD, Freudzon M, Golubets K, Gibson JF, Filler RB, et al. Langerhans Cells Facilitate UVB-Induced Epidermal Carcinogenesis. J Invest Dermatol 2015;135(11):2824-33.

Li XY, Moesta AK, Xiao C, Nakamura K, Casey M, Zhang H, et al. Targeting CD39 in Cancer Reveals an Extracellular ATP- and Inflammasome-Driven Tumor Immunity. Cancer Discov 2019;9(12):1754-73.

Liu Q, Wang G, Chen Y, Li G, Yang D, Kang J. A miR-590/Acvr2a/Rad51b axis regulates DNA damage repair during mESC proliferation. Stem Cell Reports 2014;3(6):1103-17.

Machida S, Takaku M, Ikura M, Sun J, Suzuki H, Kobayashi W, et al. Nap1 stimulates homologous recombination by RAD51 and RAD54 in higher-ordered chromatin containing histone H1. Sci Rep 2014;4:4863.

MacLeod AS RR, Corriden R, Garijo O, Ye I, and Havran WL. Skin-Resident T Cells Sense Ultraviolet Radiation-Induced Injury and Contribute to DNA Repair. Journal of Immunology 2014;192(12):5695-702.

Majewski S, Jantschitsch C, Maeda A, Schwarz T, Schwarz A. IL-23 antagonizes UVR-induced immunosuppression through two mechanisms: reduction of UVR-induced DNA damage and inhibition of UVR-induced regulatory T cells. J Invest Dermatol 2010;130(2):554-62.

Mandapathil M, Boduc M, Roessler M, Guldner C, Walliczek-Dworschak U, Mandic R. Ectonucleotidase CD39 expression in regional metastases in head and neck cancer. Acta Otolaryngol 2018;138(4):428-32.

Mandapathil M, Szczepanski MJ, Szajnik M, Ren J, Lenzner DE, Jackson EK, et al. Increased ectonucleotidase expression and activity in regulatory T cells of patients with head and neck cancer. Clin Cancer Res 2009;15(20):6348-57.

Marti TM, Hefner E, Feeney L, Natale V, Cleaver JE. H2AX phosphorylation within the G1 phase after UV irradiation depends on nucleotide excision repair and not DNA double-strand breaks. Proc Natl Acad Sci U S A 2006;103(26):9891-6.

Mascanfroni ID, Yeste A, Vieira SM, Burns EJ, Patel B, Sloma I, et al. IL-27 acts on DCs to suppress the T cell response and autoimmunity by inducing expression of the immunoregulatory molecule CD39. Nat Immunol 2013;14(10):1054-63.

Mazurkiewicz J, Kepert JF, Rippe K. On the mechanism of nucleosome assembly by histone chaperone NAP1. J Biol Chem 2006;281(24):16462-72.

McGovern N, Schlitzer A, Gunawan M, Jardine L, Shin A, Poyner E, et al. Human dermal CD14(+) cells are a transient population of monocyte-derived macrophages. Immunity 2014;41(3):465-77.

Mizumoto N, Kumamoto T, Robson SC, Sevigny J, Matsue H, Enjyoji K, et al. CD39 is the dominant Langerhans cell-associated ecto-NTPDase: modulatory roles in inflammation and immune responsiveness. Nat Med 2002;8(4):358-65.

Modi BG, Neustadter J, Binda E, Lewis J, Filler RB, Roberts SJ, et al. Langerhans cells facilitate epithelial DNA damage and squamous cell carcinoma. Science 2012;335(6064):104-8.

Mohme M, Schliffke S, Maire CL, Runger A, Glau L, Mende KC, et al. Immunophenotyping of Newly Diagnosed and Recurrent Glioblastoma Defines Distinct Immune Exhaustion Profiles in Peripheral and Tumor-infiltrating Lymphocytes. Clin Cancer Res 2018;24(17):4187-200.

Padilla RS, Sebastian S, Jiang Z, Nindl I, Larson R. Gene expression patterns of normal human skin, actinic keratosis, and squamous cell carcinoma: a spectrum of disease progression. Arch Dermatol 2010;146(3):288-93.

Palomera-Sanchez Z, Zurita M. Open, repair and close again: chromatin dynamics and the response to UV-induced DNA damage. DNA Repair (Amst) 2011;10(2):119-25.

Pardoll DM. The blockade of immune checkpoints in cancer immunotherapy. Nature reviews 2012;12(4):252-64.

Paull TT, Rogakou EP, Yamazaki V, Kirchgessner CU, Gellert M, Bonner WM. A critical role for histone H2AX in recruitment of repair factors to nuclear foci after DNA damage. Curr Biol 2000;10(15):886-95.

Peleli M, Fredholm BB, Sobrevia L, Carlstrom M. Pharmacological targeting of adenosine receptor signaling. Mol Aspects Med 2017;55:4-8.

Pflanz S, Hibbert L, Mattson J, Rosales R, Vaisberg E, Bazan JF, et al. WSX-1 and glycoprotein 130 constitute a signal-transducing receptor for IL-27. J Immunol 2004;172(4):2225-31.

Que SKT, Zwald FO, Schmults CD. Cutaneous squamous cell carcinoma: Incidence, risk factors, diagnosis, and staging. J Am Acad Dermatol 2018;78(2):237-47.

Rogakou EP, Pilch DR, Orr AH, Ivanova VS, Bonner WM. DNA double-stranded breaks induce histone H2AX phosphorylation on serine 139. J Biol Chem 1998;273(10):5858-68.

Rokunohe D, Ratnakumar K, Kohrn BF, Loubet-Senear K, Shen J, Loeb LA, et al. 748 Duplex sequencing reveals the effects of caffeine on reducing UV-induced mutations of cancer-relevant genes. Journal of Investigative Dermatology 2019;139(5):S129.

Sanchez-Tena S, Cubillos-Rojas M, Schneider T, Rosa JL. Functional and pathological relevance of HERC family proteins: a decade later. Cell Mol Life Sci 2016;73(10):1955-68.

Schmitt S, Johnson TS, Karakhanova S, Naher H, Mahnke K, Enk AH. Extracorporeal photophoresis augments function of CD4+CD25+FoxP3+ regulatory T cells by triggering adenosine production. Transplantation 2009;88(3):411-6.

Schuler PJ, Schilling B, Harasymczuk M, Hoffmann TK, Johnson J, Lang S, et al. Phenotypic and functional characteristics of CD4+ CD39+ FOXP3+ and CD4+ CD39+ FOXP3neg T-cell subsets in cancer patients. Eur J Immunol 2012;42(7):1876-85.

Sekar D, Hahn C, Brune B, Roberts E, Weigert A. Apoptotic tumor cells induce IL-27 release from human DCs to activate Treg cells that express CD69 and attenuate cytotoxicity. Eur J Immunol 2012;42(6):1585-98.

Sheikh MS, Huang Y, Fernandez-Salas EA, El-Deiry WS, Friess H, Amundson S, et al. The antiapoptotic decoy receptor TRID/TRAIL-R3 is a p53-regulated DNA damage-inducible gene that is overexpressed in primary tumors of the gastrointestinal tract. Oncogene 1999;18(28):4153-9.

Shen Y, Ma J, Yan R, Ling H, Li X, Yang W, et al. Impaired self-renewal and increased colitis and dysplastic lesions in colonic mucosa of AKR1B8-deficient mice. Clin Cancer Res 2015;21(6):1466-76.

Thyss R, Virolle V, Imbert V, Peyron JF, Aberdam D, Virolle T. NF-kappaB/Egr-1/Gadd45 are sequentially activated upon UVB irradiation to mediate epidermal cell death. EMBO J 2005;24(1):128-37.

Toda M, Wang L, Ogura S, Torii M, Kurachi M, Kakimi K, et al. UV irradiation of immunized mice induces type 1 regulatory T cells that suppress tumor antigen specific cytotoxic T lymphocyte responses. Int J Cancer 2011;129(5):1126-36.

Tsukimoto M. Purinergic Signaling Is a Novel Mechanism of the Cellular Response to Ionizing Radiation. Biol Pharm Bull 2015;38(7):951-9.

Vigano S, Alatzoglou D, Irving M, Menetrier-Caux C, Caux C, Romero P, et al. Targeting Adenosine in Cancer Immunotherapy to Enhance T-Cell Function. Front Immunol 2019;10:925.

Vogt TJ, Gevensleben H, Dietrich J, Kristiansen G, Bootz F, Landsberg J, et al. Detailed analysis of adenosine A2a receptor (ADORA2A) and CD73 (5'-nucleotidase, ecto, NT5E) methylation and gene expression in head and neck squamous cell carcinoma patients. Oncoimmunology 2018;7(8):e1452579.

Wen LT, Knowles AF. Extracellular ATP and adenosine induce cell apoptosis of human hepatoma Li-7A cells via the A3 adenosine receptor. British journal of pharmacology 2003;140(6):1009-18.

Xia S, Wei J, Wang J, Sun H, Zheng W, Li Y, et al. A requirement of dendritic cell-derived interleukin-27 for the tumor infiltration of regulatory T cells. J Leukoc Biol 2014.

Yan J, Li XY, Roman Aguilera A, Xiao C, Jacoberger-Foissac C, Nowlan B, et al. Control of Metastases via Myeloid CD39 and NK Cell Effector Function. Cancer Immunol Res 2020;8(3):356-67.

Yang B, Suwanpradid J, Sanchez-Lagunes R, Choi HW, Hoang P, Wang D, et al. IL-27 Facilitates Skin Wound Healing through Induction of Epidermal Proliferation and Host Defense. J Invest Dermatol 2017;137(5):1166-75.

Yang C, Zang W, Tang Z, Ji Y, Xu R, Yang Y, et al. A20/TNFAIP3 Regulates the DNA Damage Response and Mediates Tumor Cell Resistance to DNA-Damaging Therapy. Cancer Res 2018;78(4):1069-82.

FIGURE LEGENDS

Figure 1. ENTPD1 expression is increased within human cSCC and correlated with metastasis.

Measurement of ectonucleotidase triphosphate diphosphodydrolase 1 (ENTPD1) expression in unmatched human normal skin (NS) and cutaneous squamous cell carcinoma (cSCC) by (A) qpCR for *ENTPD1* mRNA (n_{NS}=8, n_{SCC}=10) and (B) detection of ENTPD1$^+$ cells by flow cytometry of fresh tissue (n_{NS}=11, n_{SCC}=13). (C) Analysis of human primary SCC for ENTPD1 expression among peritumoral immune cells via immunohistochemistry (IHC) in tumors that metastasized ((+) met, n=54) vs those that did not ((-) met, n=51). (D) ENTPD1 expression within CD45$^+$ and CD45$^-$ populations of cells by flow cytometry of fresh tissue (n_{NS}=11, n_{SCC}=13). (E) In vivo expression of ENTPD1 within the stroma of cSCC. Dotted lines indicate the epidermal-dermal junction (scale bar = 200 μm). (F) ENTPD1 expression by CD3$^+$ T-cells (n=13) isolated from human cSCC, peritumoral non-lesional (NL) and blood. Each data point represents one patient sample. *P* values determined by unpaired *t* test.

Figure 2. Human cSCCs are enriched for ENTPD1$^+$ memory T cells.

ENTPD1 expression among (**A**) CD8+, (**B**) CD4+ FoxP3-, and (**C, D, E**) CD4+ FoxP3+ T-cells isolated from human SCC, perilesional skin (NL), and blood (n=13). % positive cells shown by flow cytometry in **A-C, E** and mean fluorescence intensity (MFI) by flow cytometry shown in **D**. Percentage of CD45RO+ cells among ENTPD1+ populations of (**F**) CD4+ and (**G**) CD8+ T cells isolated from human SCC, perilesional skin (NL), and blood (n=7). (**H**) CD45RO+ENTPD1+ cells are enriched among CD4+FoxP3+ T cells in cSCC compared to NL and blood (n=7). (**I, J**) Representative flow cytometry analysis of CD45RO, FoxP3 and ENTPD1 expression in cells

isolated from human SCC, perilesional skin (NL), and blood. *P* values determined by Tukey's multiple comparisons test.

Figure 3. ENTPD1+ T cells express cutaneous lymphocyte antigen (CLA).

(**A**) Representative flow cytometry of analysis of total T cells isolated from human cSCC showing CLA expression within the $ENTPD1^{+}$ vs $ENTPD1^{-}$ populations. CLA expression among (**B**) CD4+ ENTPD1+ and (**C**) CD8+ENTPD1+ T cells isolated from human SCC, perilesional skin (NL), and blood (n=12). *P* values determined by Tukey's multiple comparisons test.

Figure 4. ENTPD1 and PD1 are co-expressed on FoxP3- T Cells.

(A) PD1 expression and (**B**) coexpression with ENTPD1 among T cells isolated from human cSCC (SCC, n=8), perilesional skin (NL, n=5)), and blood (n=3). (**C**) PD1 and ENTPD1 co-expression within FoxP3- and FoxP3+ populations among T cells isolated from human SCC, perilesional skin (NL), and blood. *P* values determined by Tukey's multiple comparisons test.

Figure 5. UV-induced ENTPD1 expression is IL-27-dependent.

(A) Representative flow cytometric analysis of IL-27A expression in CD14+ cells in healthy normal skin (NS) and SCC. Representative immunoflourescence microscopy of IL-27A expression in (**B**) NS and (**C**) SCC (scale bar = 500 μm). (**D**) Representative co-staining for IL-27A and CD209 in a human SCC sample (scale bar = 200 μm). (**E**) Relative expression of ENTPD1 and FoxP3 in human skin-derived T cells from healthy donors after stimulation with rhIL-27. (**F**) ENTPD1 expression by qPCR of mouse skin harvested from WT and $IL\text{-}27RA^{-/-}$

mice 18 hours after UVB exposure. (**G**) %ENTPD1^{+} cells by flow cytometry in mouse skin harvested from WT and IL-27RA$^{-/-}$ mice one day after UVB exposure ($n_{WT, mock}$=2, $n_{WT, UVB}$=3, $n_{IL27RA-/-, mock}$=3, $n_{IL27RA-/-, UVB}$=2). Error bars represent SEM. *P* value determined by unpaired t test.

Figure 6. UV-induced DNA damage is potentiated by IL-27/ETNPD1 and may be mediated by NAP1L2.

(**A**) Human keratinocytes were cultured with acellular medium (n=3), anti-CD3 stimulated skin-resident T cells (n=4), or IL-27A primed (100 ng/ml) and anti-CD3 stimulated skin-resident T cells (n=3) followed by UVB irradiation and measurement of DNA damage by quantification of γH2AX after 24 hours. (**B**) Epidermal sheets isolated from the ears of WT, ENTPD1$^{-/-}$, and IL27ra$^{-/-}$ C57BL/6 mice were exposed to UVB irradiation with or without recombinant IL-27A treatment followed by quantification of γH2AX^{+} after 24 hours ($n_{WT, UVB}$=4, $n_{WT, UVB+rIL27}$=3, $n_{ENTPD1-/-, UVB}$=3, $n_{ENTPD1-/-, UVB+rIL27}$=3, $n_{IL27RA-/-, UVB}$=3, $n_{IL27RA-/-, UVB+rIL27}$=3). Co-localization of ENTPD1^{+} and γH2AX^{+} cells in (**C**) cSCC (representative of n=7) and (**D**) nonlesional skin by immunofluorescence microscopy (scale bar = 1 mm and 200 μm for low and high power images, respectively). (**E**) Heat map of the top 49 most significant probes in normal human keratinocytes treated with vehicle or 10 μM adenosine for 24 hours. Normalized gene expression has been z-score transformed. Samples and genes were each clustered using correlation distance with complete linkage. Measurement of NAP1L2 expression in A431 SCC cell line treated with vehicle or 10 μM adenosine via (**F**) qPCR for *NAP1L2* mRNA (n=3) at 24 hours or (**G**) immunohistochemistry for NAP1L2 protein at 48 hours (scale bar = 20 μm). (**H**) Measurement of DNA damage via %γH2AX^{+} cells at 2, 24, and 36 hours after UVB irradiation of

keratinocytes with or without siRNA knockdown of NAP1L2 (n=3 distinct NHEK donors depicted by distinct symbols). Error bars represent SEM. *P* value determined by unpaired t test in A, B, F and paired t test in H.

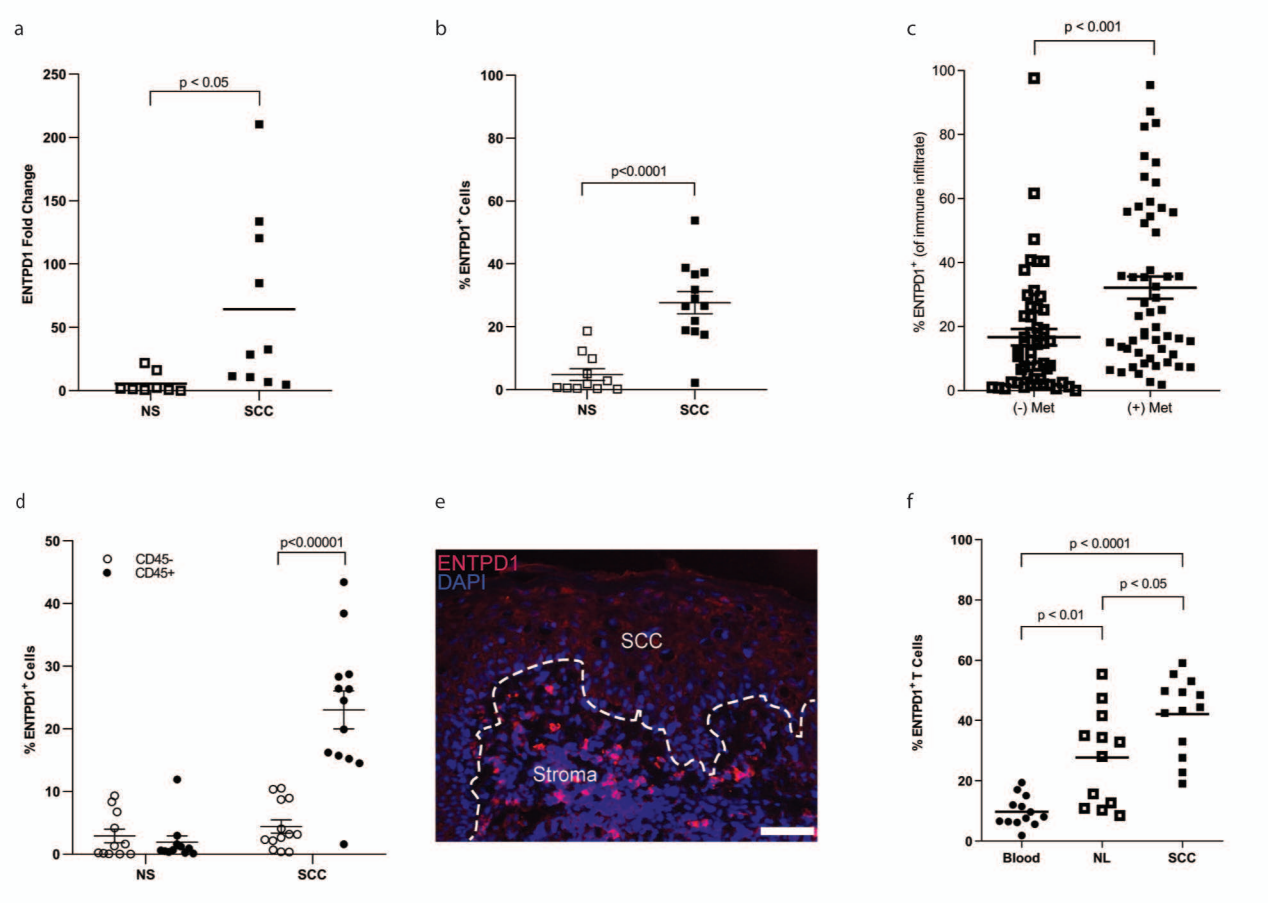
a
ENTPD1 Fold Change
p < 0.05
NS
SCC
b
% ENTPD1+ Cells
p<0.0001
NS
SCC
c
% ENTPD1+ (of immune infiltrate)
p < 0.001
(-) Met
(+) Met
d
% ENTPD1+ Cells
CD45-
CD45+
p<0.00001
NS
SCC
e
ENTPD1
DAPI
SCC
Stroma
f
% ENTPD1+ T Cells
p < 0.0001
p < 0.05
p < 0.01
Blood
NL
SCC

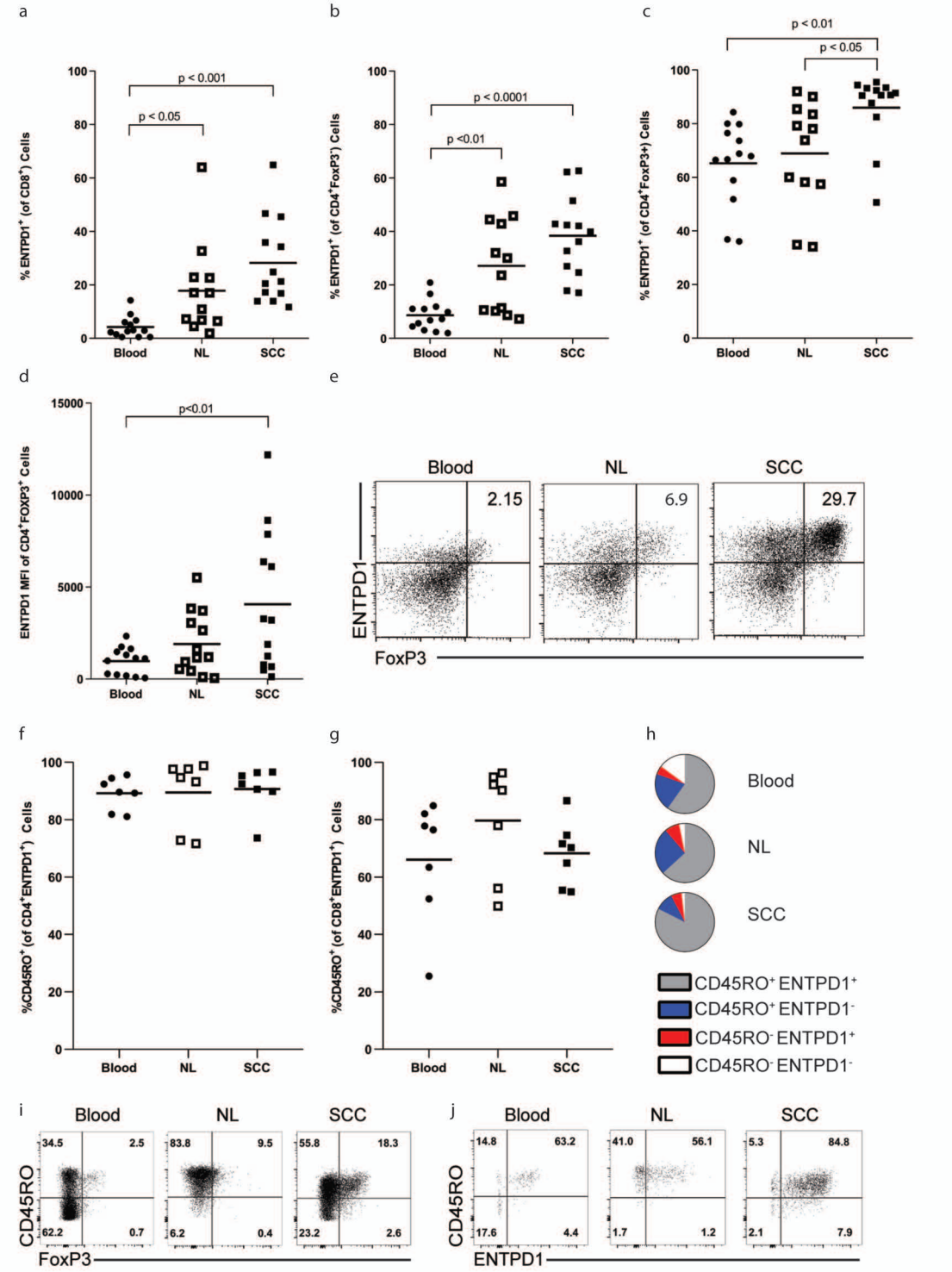
a
% ENTPD1+ (of CD8+) Cells
p < 0.001
p < 0.05
Blood
NL
SCC
b
% ENTPD1+ (of CD4+FoxP3-) Cells
p < 0.0001
p <0.01
c
% ENTPD1+ (of CD4+FoxP3+) Cells
p < 0.01
p < 0.05
d
ENTPD1 MFI of CD4+FOXP3+ Cells
p<0.01
e
Blood
NL
SCC
2.15
6.9
29.7
ENTPD1
FoxP3
f
%CD45RO+ (of CD4+ENTPD1+) Cells
g
%CD45RO+ (of CD8+ENTPD1+) Cells
h
Blood
NL
SCC
CD45RO+ ENTPD1+
CD45RO+ ENTPD1-
CD45RO- ENTPD1+
CD45RO- ENTPD1-
i
Blood
NL
SCC
34.5
2.5
62.2
0.7
83.8
9.5
6.2
0.4
55.8
18.3
23.2
2.6
CD45RO
FoxP3
j
Blood
NL
SCC
14.8
63.2
17.6
4.4
41.0
56.1
1.7
1.2
5.3
84.8
2.1
7.9
CD45RO
ENTPD1

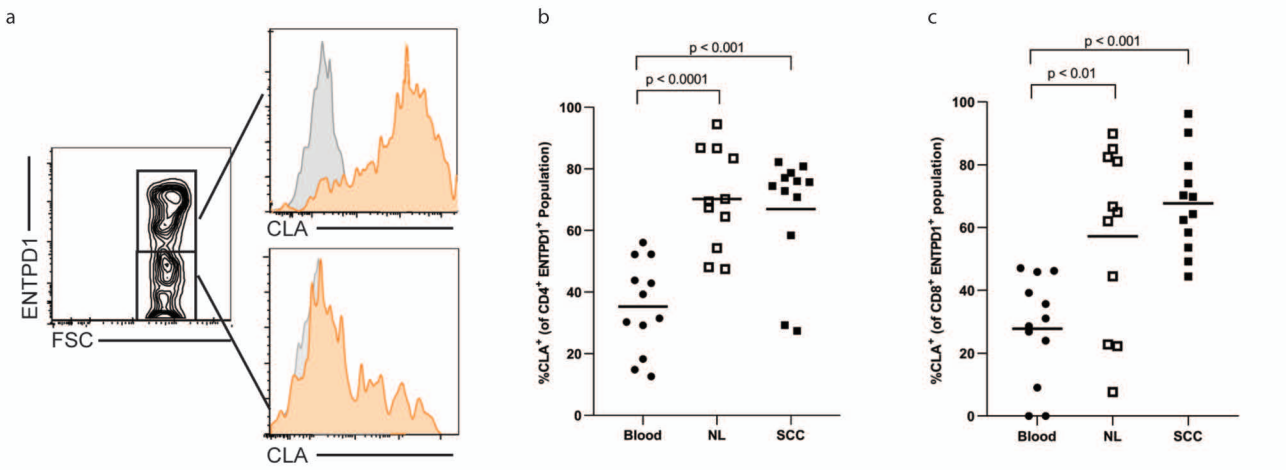
a
ENTPD1
FSC
CLA
CLA
b
p < 0.001
p < 0.0001
%CLA+ (of CD4+ ENTPD1+ Population)
100
80
60
40
20
0
Blood
NL
SCC
c
p < 0.001
p < 0.01
%CLA+ (of CD8+ ENTPD1+ population)
100
80
60
40
20
0
Blood
NL
SCC

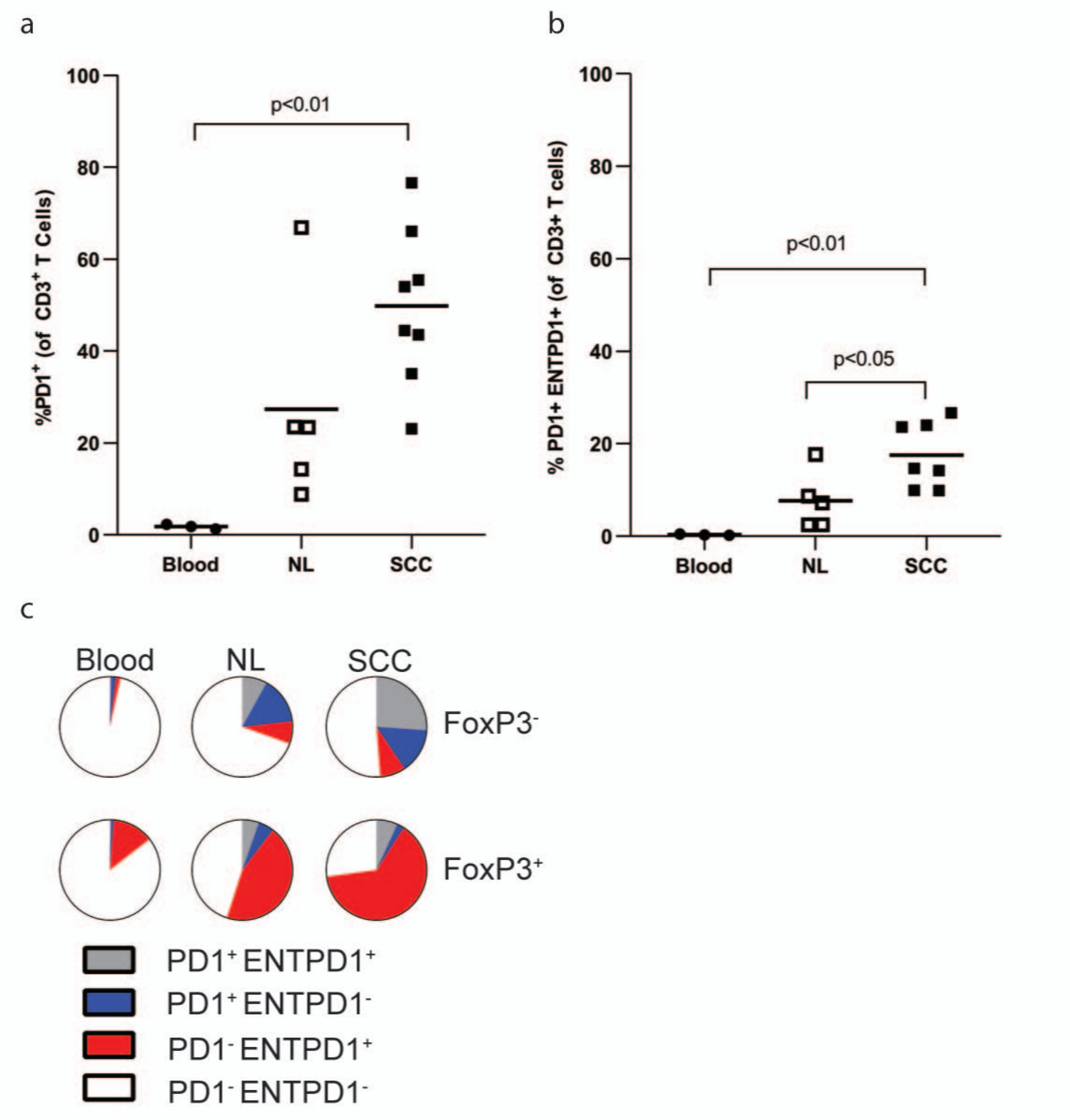
a
100
80
60
40
20
0
%PD1+ (of CD3+ T Cells)
p<0.01
Blood
NL
SCC
b
100
80
60
40
20
0
% PD1+ ENTPD1+ (of CD3+ T cells)
p<0.01
p<0.05
Blood
NL
SCC
c
Blood
NL
SCC
FoxP3-
FoxP3+
PD1+ ENTPD1+
PD1+ ENTPD1-
PD1- ENTPD1+
PD1- ENTPD1-

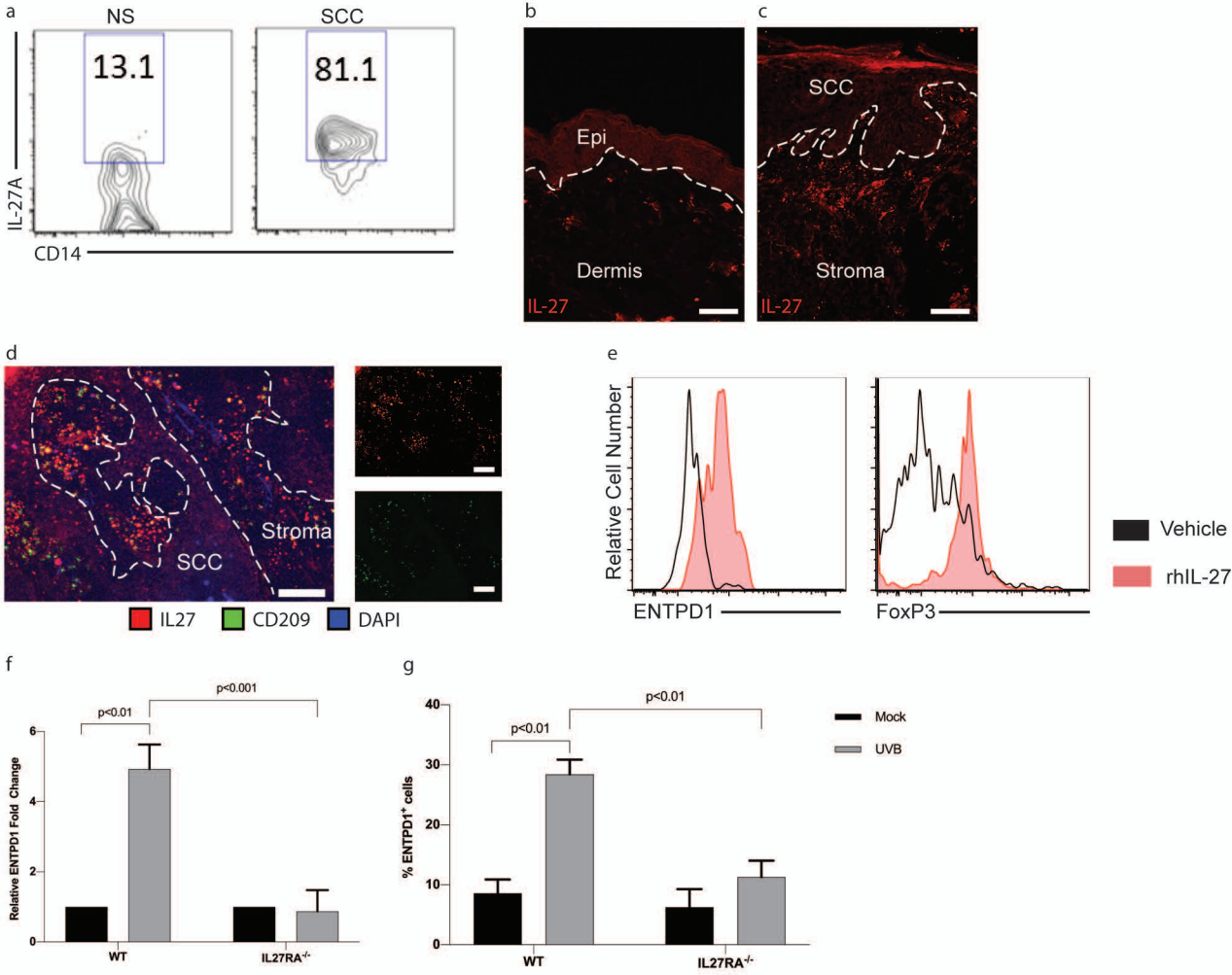
a
NS
SCC
13.1
81.1
IL-27A
CD14
b
Epi
Dermis
IL-27
c
SCC
Stroma
IL-27
d
Stroma
SCC
IL27
CD209
DAPI
e
Relative Cell Number
ENTPD1
FoxP3
Vehicle
rhIL-27
f
p<0.01
p<0.001
Relative ENTPD1 Fold Change
WT
IL27RA-/-
g
p<0.01
p<0.01
% ENTPD1+ cells
Mock
UVB
WT
IL27RA-/-

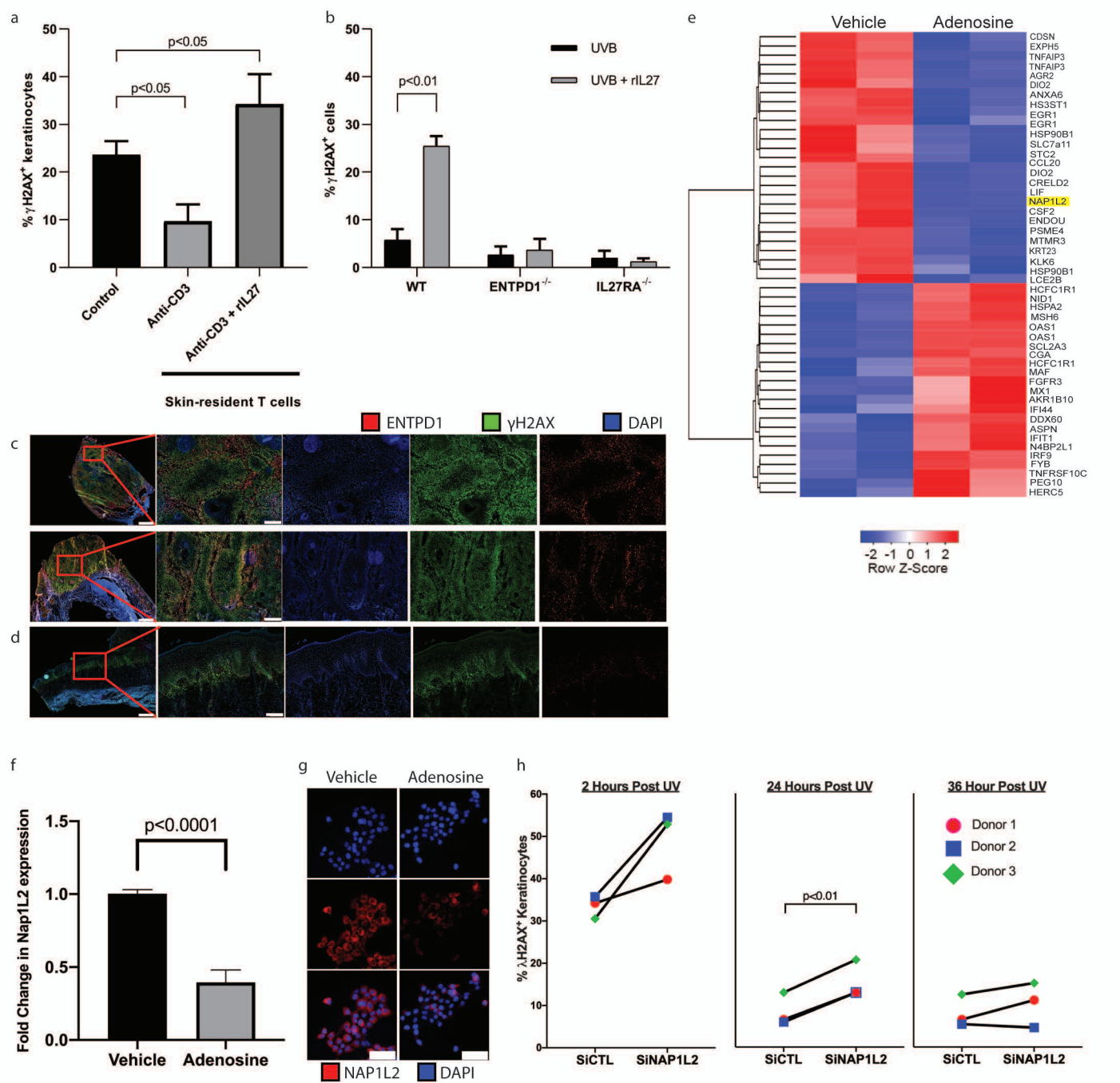
a
% γH2AX+ keratinocytes
p<0.05
p<0.05
Control
Anti-CD3
Anti-CD3 + rIL27
Skin-resident T cells
b
% γH2AX+ cells
UVB
UVB + rIL27
p<0.01
WT
ENTPD1-/-
IL27RA-/-
e
Vehicle
Adenosine
CDSN
EXPH5
TNFAIP3
TNFAIP3
AGR2
DIO2
ANXA6
HS3ST1
EGR1
EGR1
HSP90B1
SLC7a11
STC2
CCL20
DIO2
CRELD2
LIF
NAP1L2
CSF2
ENDOU
PSME4
MTMR3
KRT23
KLK6
HSP90B1
LCE2B
HCFC1R1
NID1
HSPA2
MSH6
OAS1
OAS1
SCL2A3
CGA
HCFC1R1
MAF
FGFR3
MX1
AKR1B10
IFI44
DDX60
ASPN
IFIT1
N4BP2L1
IRF9
FYB
TNFRSF10C
PEG10
HERC5
-2 -1 0 1 2
Row Z-Score
c
ENTPD1
γH2AX
DAPI
d
f
Fold Change in Nap1L2 expression
p<0.0001
Vehicle
Adenosine
g
Vehicle
Adenosine
NAP1L2
DAPI
h
2 Hours Post UV
24 Hours Post UV
36 Hour Post UV
% λH2AX+ Keratinocytes
p<0.01
Donor 1
Donor 2
Donor 3
SiCTL
SiNAP1L2
SiCTL
SiNAP1L2
SiCTL
SiNAP1L2

SUPPLEMENTAL FIGURE LEGENDS

<u>Supplementary Figure 1</u>. ENTPD1 expression is increased within human cSCC compared to normal skin

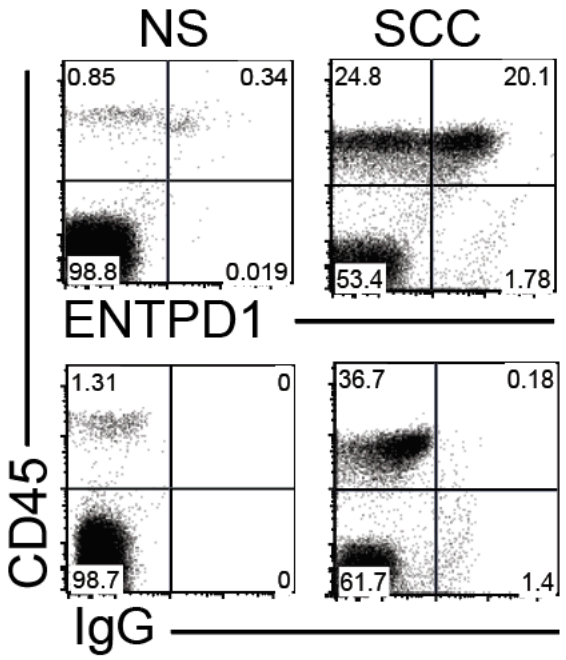

Representative example of ENTPD1 expression in unmatched human normal skin (NS, n=11) and cutaneous squamous cell carcinoma (SCC, n=13).

<u>Supplementary Figure 2.</u> ENTPD1 and CD73 expression among T cells and macrophages in cutaneous squamous cell carcinoma, peritumoral skin, and peripheral blood.

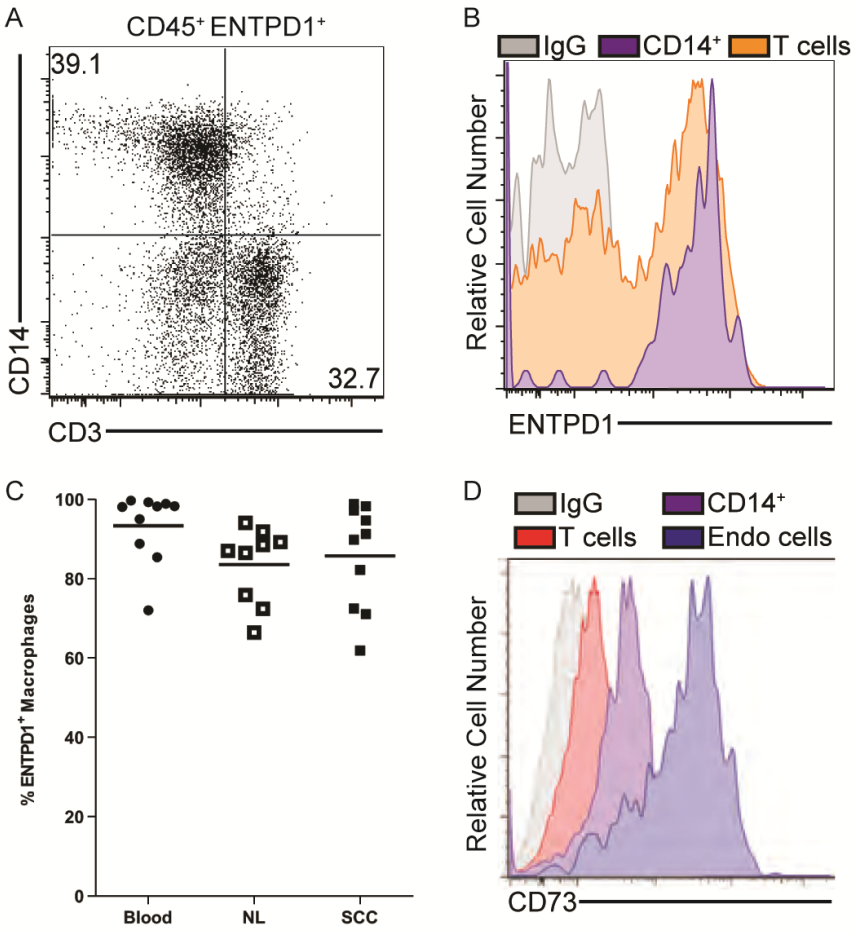

(**A, B**) Representative example of $CD45^+$ $ENTPD1^+$ cells from human cSCC that are composed of $CD3^+$ T-cell and $CD14^+$ macrophage populations. (**C**) ENTPD1 expression by $CD14^+$ macrophages (n=9) isolated from human cSCC (SCC), peritumoral non-lesional (NL) skin and blood. (**D**) Representative expression of CD73, a different ectonucleotidase, among different peritumoral cell types. *P* values determined by Tukey's multiple comparisons test.

<u>Supplementary Figure 3</u>. ENTPD1 and CD73 expression by epidermal and dermal dendritic cells and macrophages.

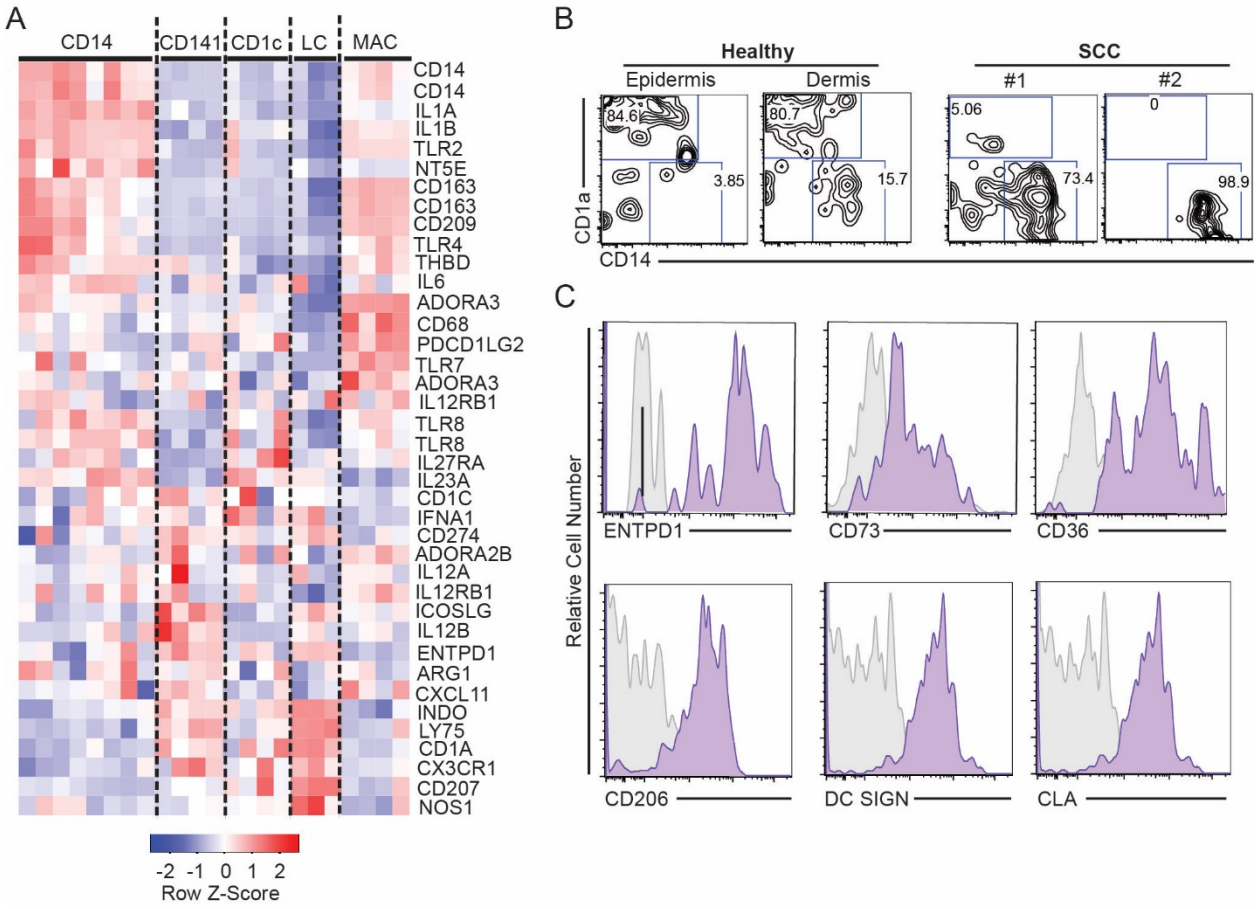

(**A**) Heat map showing several target genes encoding innate immunity genes including Toll-like receptors (TLR), cytokines and their receptors. Normalized gene expression data was z-score transformed. Datasets from Schlitzer et al. (GSE35459) and McGovern et al. (GSE60317) were downloaded from GEO. (B) Flow cytometry analysis of CD1a and CD14 expression on epidermal and dermal cell suspensions from healthy normal skin and cSCC skin. (C) Flow cytometry analysis of CD14+ cells isolated from human cSCC express ENTPD1 and various surface markers. IgG controls depicted in grey. Results representative of 3-4 patient samples.

<u>Supplementary Figure 4</u>. ENTPD1 expression co-localizes with γH2AX$^+$ cells in cSCC and nonlesional skin.

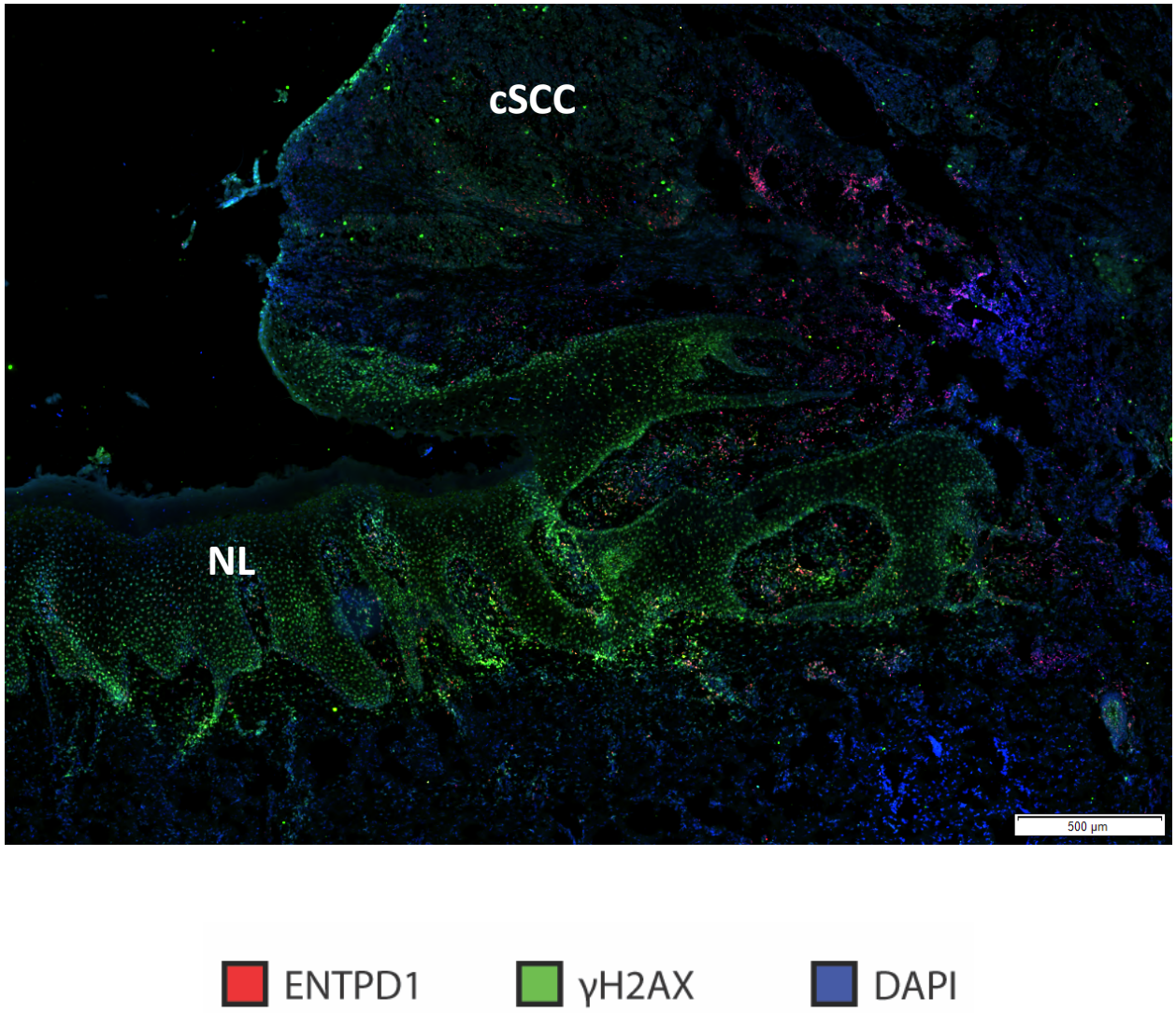

ENTPD1 expression co-localizes with areas of high DNA damage as measured by γH2AX$^+$ within cSCCs and peritumoral nonlesional (NL) skin. ENTPD1 expression is higher within the lesional tissue.

<u>Supplementary Figure 5</u>. Extracellular ATP metabolites including adenosine are increased in human cutaneous squamous cell carcinoma.

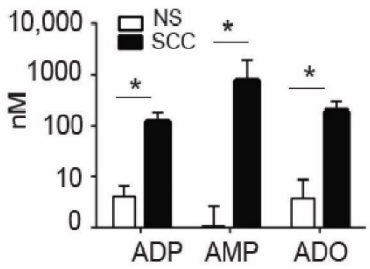

Measurements of adenosine diphosphate (ADP), adenosine monophosphate (AMP), and adenosine (ADO) from supernatants of SCC and normal skin (NS) by tandem-mass spectrometry. *P<0.05 as determined by two-tailed Student's t-test.

<u>Supplementary Figure 6.</u> UV radiation-induced ENTPD1 expression in cutaneous squamous cell carcinoma inhibits DNA damage repair via purinergic signaling and is associated with metastasis. UV radiation induces keratinocyte damage and IL27-mediated upregulation of ENTPD1 expression on cells, including regulatory T cells, which results in the increased concentration of extracellular adenosine. Our studies show that increased extracellular adenosine downregulates expression of NAP1L2, inhibiting effective DNA damage repair and thereby promoting tumorigenesis. We also show that ENTPD1 expressing tumors are more likely to metastasize.

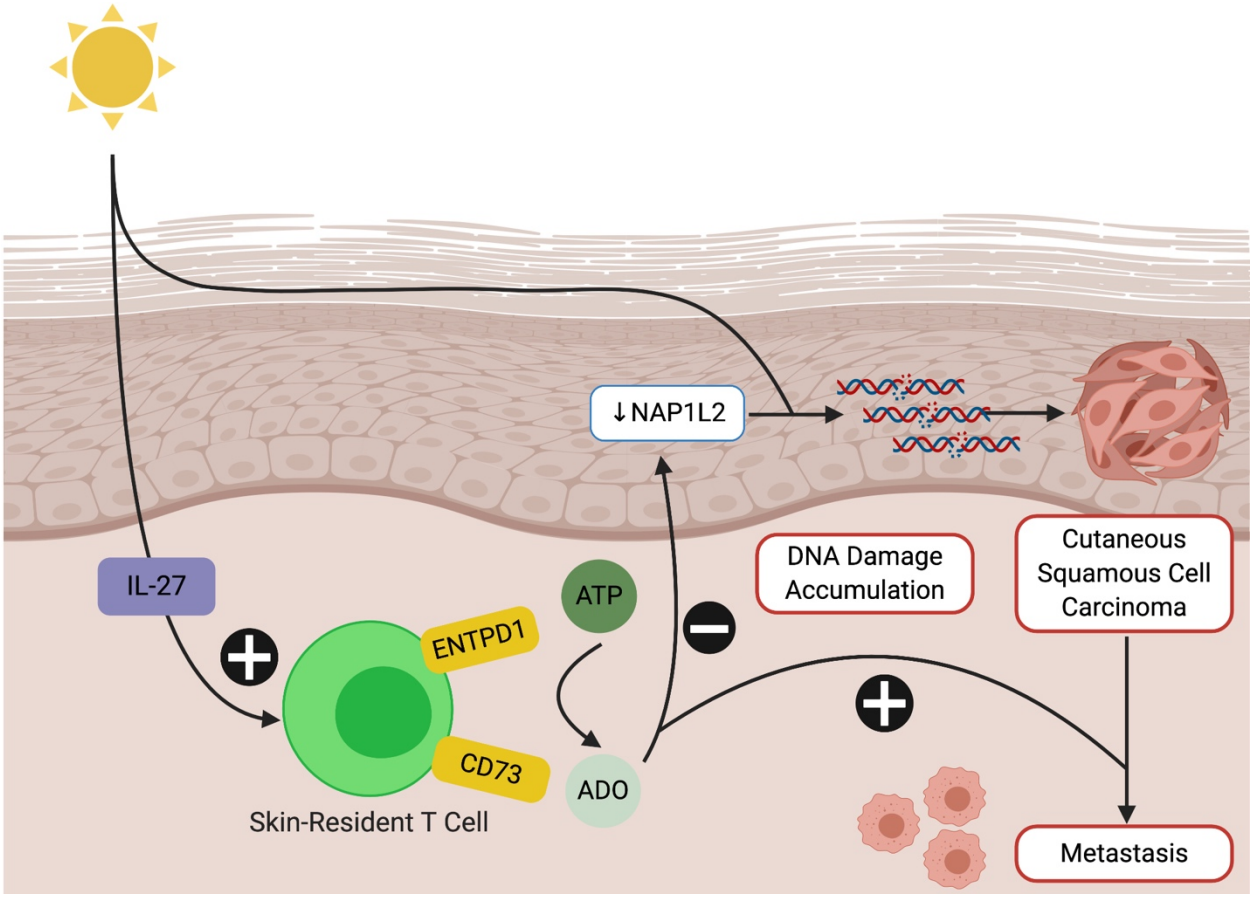

SUPPLEMENTAL MATERIALS AND METHODS

Human tissue and cells. All human samples for this study were obtained according to protocols approved by the IRB at Duke University, University of Southampton (UK), and Scripps Research Institute, CA. Written informed consent was received from patients as required by the relevant protocols.

Normal skin samples were obtained from otherwise discarded tissue from procedures performed at Duke University, Scripps Green Hospital, and Scripps Clinic Ambulatory Surgical Center, Carmel Valley. SCC samples were collected following excision performed at Duke University, Scripps Clinic, and University of Southampton. Peripheral blood mononuclear cells were isolated from venous patient blood by centrifugation with Lymphoprep (Axis-Shield).

Normal human keratinocytes were purchased from (Cascade Biologics) and grown in serum-free EpiLife cell culture medium containing 0.06 mM Ca2+, EpiLife Defined Growth Supplement, 50 U/ml penicillin and 50 mg/ml streptomycin, maintained for up to five passages, and used at approximately 75-80% confluence for experiments. A431 SCC cell line cells were purchased from ATCC (CRL-1555) and grown in DMEM with 10% FBS. For some experiments, cells were stimulated in 2-4 well chamber slides (Lab-Tek) with cell-free supernatants from anti-CD3-activated skin-resident T cells (T cell supernatants, TC sups) and were irradiated with 10 mJ/cm^2 UVB before immunohistochemical analyses. For some experiments, cell culture medium was collected from from either UVB-treated or non-treated keratinocytes and used for stimulation of human skin-resident T cells. Tissue samples from normal donors were used to obtain skin-resident T cell explant cultures as previously described (MacLeod AS, 2014) with the exception that cells were kept in complete RPMI 1640 medium with 10% FCS without cytokines. For experiments where T cell supernatants were used, T cells were stimulated in keratinocyte EpiLife

medium (Cascade Biologics). Anti-CD3 (OKT3, Biolegend) was immobilized to individual wells of 96-well flat-bottom plates. In some experiments, cells were treated with 10 μM adenosine (Sigma) diluted in growth media.

Mouse experiments. All mice were bred and studies performed at Duke University and The Scripps Research Institute according to protocols approved by Institutional Animal Care and Use Committees (IACUC) guidelines.

For some experiments, mice were irradiated with an EB-280C/12 UVB lamp (100 mJ/cm^{-2}, Spectroline, predominant emission 312nm, 270-390nm emission range) after removing their back hair.

Epidermal, dermal and whole skin cell suspensions were freshly isolated from mouse skin as previously described (MacLeod AS, 2014) and were cultured in complete RPMI 1640 containing 10% FCS.

For analyses of γH2AX in mouse ears, ears were excised, separated into dorsal and ventral ear halves as previously described (MacLeod AS, 2014, MacLeod et al., 2013), and were floated epidermis side-up in complete DMEM (Dulbeccos) with 10% FCS and were irradiated with 100 mJ/cm^2 UVB. Sections were visualized using a Nikon Eclipse E800 microscope and digital images were acquired with a Zeiss AxioCam HRc camera.

Liquid chromatography – electrospray tandem mass spectrometry (LC-ESI-MS/MS).

ATP, ADP, AMP, and ADO measurement was performed by the Duke Cancer Institute PK/PD Core laboratory using LC-ESI-MS/MS. Pure standards of ADO, ADO13C5, AMP, ADP, ATP (Sigma-Aldrich) and ATP15N5 (TRC) were of analytical purity. Methods from Goutiera et al. (Goutier et al., 2010) were modified to accommodate additional metabolites and available

instrumentation. Briefly, 100 μL of cell-free supernatants from SCC in NaCl was combined with 200 μL of mobile phase A (described below) and 10 μL of 10 μM of solution of ADO13C5 and ATP15N5 internal standards in mobile phase A, vortexed, and 10 μL directly injected into the LC-ESI-MS/MS system. Chromatographic separation was accomplished on a Shimadzu 20A series HPLC (LC) equipped with ZIC® -pHILIC (5 μm, 150×4.6 mm) column (SeQuant, AB, Sweden). Mobile phase A consisted of 10 mM ammonium bicarbonate buffer adjusted to pH 9.4 with ammonium hydroxide in 20% acetonitrile in HPLC grade water. Mobile phase B was acetonitrile. Flow rate was 0.8 mL/min. Electrospray ionization tandem-mass spectrometry (ESI-MS/MS) detection was performed on an Applied Biosystems/SCIEX API 4000 QTrap instrument. The following m/z MS/MS transitions were followed: 266/133.8 (ADO), 271/133.8 (ADO13C5, used as internal standard for ADO and AMP), 346/150.8 (AMP), 426/158.8 (ADP), 506/158.8 (ATP) and 511/158.8 (ATP15N5, used as int. std. for ADP and ATP). Calibration samples containing each analyte in the range of 3.9 nM (LLOQ) - 1 μM were run before and after each batch of study samples. Linear relationship signal (analyte/int.standard) versus nominal concentration was confirmed for all the analytes and used for quantification.

REFERENCES

Goutier W, Spaans PA, van der Neut MA, McCreary AC, Reinders JH. Development and application of an LC-MS/MS method for measuring the effect of (partial) agonists on cAMP accumulation in vitro. J Neurosci Methods 2010;188(1):24-31.

MacLeod AS RR, Corriden R, Garijo O, Ye I, and Havran WL. Skin-Resident T Cells Sense Ultraviolet Radiation-Induced Injury and Contribute to DNA Repair. Journal of Immunology 2014;192(12):5695-702.

MacLeod AS, Hemmers S, Garijo O, Chabod M, Mowen K, Witherden DA, et al. Dendritic epidermal T cells regulate skin antimicrobial barrier function. J Clin Invest 2013;123(10):4364-74.